Earth Surf. Dynam. Discuss., 3, 1445–1508, 2015
www.earth-surf-dynam-discuss.net/3/1445/2015/
doi:10.5194/esurfd-3-1445-2015

Earth Surface Dynamics Discussions
Open Access
EGU

Image-based surface reconstruction in geomorphometry – merits, limits and developments of a promising tool for geoscientists

A. Eltner[1], A. Kaiser[2], C. Castillo[3], G. Rock[4], F. Neugirg[5], and A. Abellan[6]

[1]Institute of Photogrammetry and Remote Sensing, Technical University Dresden, Dresden, Germany
[2]Soil and Water Conservation Unit, Technical University Freiberg, Freiberg, Germany
[3]Dep. of Rural Engineering, University of Cordoba, Cordoba, Spain
[4]Dep. of Environmental Remote Sensing and Geomatics, University of Trier, Trier, Germany
[5]Dep. of Physical Geography, Catholic University Eichstätt-Ingolstadt, Eichstätt-Ingolstadt, Germany
[6]Risk Analysis Group, Institute of Earth Sciences, University of Lausanne, Lausanne, Switzerland

Received: 1 December 2015 – Accepted: 3 December 2015 – Published: 15 December 2015
Correspondence to: A. Eltner (anette.eltner@tu-dresden.de)
Published by Copernicus Publications on behalf of the European Geosciences Union.

Abstract

Photogrammetry and geosciences are closely linked since the late 19th century. Today, a wide range of commercial and open-source software enable non-experts users to obtain high-quality 3-D datasets of the environment, which was formerly reserved to remote sensing experts, geodesists or owners of cost-intensive metric airborne imaging systems. Complex tridimensional geomorphological features can be easily reconstructed from images captured with consumer grade cameras. Furthermore, rapid developments in UAV technology allow for high quality aerial surveying and orthophotography generation at a relatively low-cost. The increasing computing capacities during the last decade, together with the development of high-performance digital sensors and the important software innovations developed by other fields of research (e.g. computer vision and visual perception) has extended the rigorous processing of stereoscopic image data to a 3-D point cloud generation from a series of non-calibrated images. Structure from motion methods offer algorithms, e.g. robust feature detectors like the scale-invariant feature transform for 2-D imagery, which allow for efficient and automatic orientation of large image sets without further data acquisition information. Nevertheless, the importance of carrying out correct fieldwork strategies, using proper camera settings, ground control points and ground truth for understanding the different sources of errors still need to be adapted in the common scientific practice.

This review manuscript intends not only to summarize the present state of published research on structure-from-motion photogrammetry applications in geomorphometry, but also to give an overview of terms and fields of application, to quantify already achieved accuracies and used scales using different strategies, to evaluate possible stagnations of current developments and to identify key future challenges. It is our belief that the identification of common errors, "bad practices" and some other valuable information in already published articles, scientific reports and book chapters may help in guiding the future use of SfM photogrammetry in geosciences.

ESURFD
3, 1445–1508, 2015

1 Introduction

Early works on projective geometries date back to more than five centuries, when scientists derived coordinates of points from several images and investigated the geometry of perspectives. Projective geometry represents the basis for the developments in photogrammetry in the late 19th century, when Aimé Laussedat experimented with terrestrial imagery as well as kites and balloons for obtaining imagery for topographic mapping (Laussedat, 1899). Rapidly, photogrammetry advanced to be an essential tool in geosciences during the last two decades and is lately gaining momentum driven by digital sensors. Simultaneously, growing computing capacities and rapid developments in computer vision lead to the promising method of Structure from Motion (SfM) that opened the way for low-cost high-resolution topography. Thus, the community using image-based 3-D reconstruction experienced a considerable growth, not only in quality and detail of the achieved results but also in the number of potential users from diverse geo-scientific disciplines.

SfM photogrammetry can be performed with images acquired with consumer grade digital cameras and is thus very flexible in its implementation. Its ease of use in regard to data processing makes it further interesting to non-experts. The diversity of possible applications led to a variety of terms used to describe SfM photogrammetry either from photogrammetric or computer vision standpoint. Thus to avoid ambiguous terminology, a short list of definitions in regard to the reviewed method is given in Table 1. In this review a series of studies that utilise the algorithmic advances of SfM are considered, i.e. no initial estimates or user interactions to generate initial estimates are needed. Furthermore, data processing is performed fully automatic but parameter settings, typical for photogrammetric tools, can be applied to optimise both accuracy and precision.

SfM photogrammetry can be applied to a vast range of temporal as well as spatial scales and resolutions up to an unprecedented level of detail, allowing for new insights into earth surface processes, i.e. 4-D reconstruction of environmental dynamics. For instance, the concept of sediment connectivity (Bracken et al., 2014) can be approached

ESURFD
3, 1445–1508, 2015

from a new perspective through varying time and space scales. Furthermore, the magnitude and frequency of events and their interaction can be evaluated from a novel point of view. Also, the possibility to reconstruct surfaces from images, captured from aerial or terrestrial perspectives, inherits the advantage to be applicable in fragile and fast changing environments.

After the suitability of SfM has been noticed for geo-scientific applications (James and Robson, 2012; Westoby et al., 2012; Fonstad et al., 2013) the number of studies utilising SfM photogrammetry has increased significantly. However, the method needs sophisticated study design and some experience in image acquisition to prevent predictable errors and to ensure good quality of the reconstructed scene. James and Robson (2012) and Micheletti et al. (2015) recommend a setup for efficient data acquisition.

A total of 61 publications are reviewed in this study. They are chosen according to the respective field of research and methodology. Only studies are included that make use of the benefits of automatic image matching algorithms and thus apply the various SfM tools. Studies that lack of full automatisation are excluded, i.e. some traditional photogrammetric software. Topic wise a line is drawn in regard to the term geosciences. The largest fraction of the reviewed articles tackles questions arising in geomorphological contexts. To account for the versatility of SfM photogrammetry, a few studies deal with plant growth on different scales (moss, crops, forest) or investigate rather exotic topics such as stalagmites or reef morphology.

This review aims to highlight the development of SfM photogrammetry as a promising tool for geoscientists:

1. The method of SfM photogrammetry is briefly summarised and algorithmic differences due to their emergence from computer vision as well as photogrammetry are clarified.

2. Different fields of applications where SfM photogrammetry led to new perceptions in geomorphometry are displayed.

3. The performance of the reviewed method is evaluated.

ESURFD
3, 1445–1508, 2015

4. And frontiers and significance of SfM photogrammetry are discussed.

2 SfM photogrammetry: state-of-the-art

Reconstruction of three-dimensional geometries from images has played an important role in the past centuries (Ducher, 1987; Collier, 2002). The production of high-resolution DEMs was and still is one of the main applications of (digital) photogrammetry. Software and hardware developments as well as the increase in computing power in the 1990s and early 2000s made aerial photogrammetric processing of large image datasets accessible to a wider community (e.g. Chandler, 1999).

Camera orientations and positions, which are usually unknown during image acquisition, have to be reconstructed to model a 3-D scene. For that purpose, photogrammetry has developed bundle block adjustment (BBA) techniques, which allowed for simultaneous determination of camera orientation and position parameters as well as 3-D object point coordinates for a large number of images. The input into the BBA are image coordinates of many tie points, usually at least nine homologous points per image. If the BBA is extended by a simultaneous calibration option, even the intrinsic camera parameters can be determined in addition to the extrinsic parameters. Furthermore, a series of ground control points can be used as input into BBA for geo-referencing the image block (e.g. Luhmann et al., 2014; Kraus, 2007; Mikhail et al., 2001).

Parallel developments in computer vision took place that try to reconstruct viewing geometries of image datasets not fulfilling the common prerequisites from digital photogrammetry, i.e. calibrated cameras and initial estimates of the image acquisition scheme. This led to the structure from motion (SfM) technique (Ullman, 1979) allowing to process large datasets and to use a combination of multiple non-metric cameras.

The typical workflow of SfM photogrammetry (e.g. Snavely et al., 2008) comprises the following steps (Fig. 1):

1. identification and matching of homologous image points in overlapping photos (image matching),

ESURFD
3, 1445–1508, 2015

2. reconstruction of the geometric image acquisition configuration and of the corresponding 3-D coordinates of matched image points (sparse point cloud) with iterative BBA,

3. dense matching of the sparse point cloud from reconstructed image network geometry.

Image matching is fully automated in SfM-tools, and different interest operators can be used to select suitable image matching points. One of the most prominent examples for these matching algorithms are both the "scale-invariant-feature-transformation-algorithm" (SIFT) and the "Speeded up robust features-algorithm" (SURF). In depth descriptions of SIFT and SURF are given by Lowe (1999) and Bay (2008). These algorithms detect features (e.g. Harris corners) that are robust to image scaling, image rotation, changes in perspective and illumination. The detected features are localised in both the spatial and frequency domain and are highly distinctive, which allows differentiating one feature from a large database of other features (Lowe, 2004; Mikolajczyk, 2005). In contrast, kernel based correlation techniques are normally used in photogrammetry, which are more precise (Grün, 2012), but more constrained in regard to image configurations. When applied to oblique imagery, these kernel based correlation techniques are outperformed by the new feature based algorithms especially designed in order to match datasets from unstructured image acquisitions (Grün, 2012).

The information of the positions of the homologous image points is then used to reconstruct the image network geometry, the 3-D object point coordinates and the internal camera geometry in an iterative BBA procedure (e.g. Pears et al., 2012). SfM photogrammetry algorithms derive initial scene geometry by a comparatively large number of common features found by the matching algorithms in one pair of images (Lowe, 2004). These extrinsic parameters are estimated usually using the "random sampling consensus" (RANSAC) – algorithm (Fischler and Bolles, 1981), insensitive to relatively high number of false matches and outliers. This initial estimation of extrinsic parame-

ESURFD
3, 1445–1508, 2015

ters is refined in an iterative least-square minimization process, which also optimizes the cameras intrinsic parameters (camera self-calibration) for every single image. In contrast to classical photogrammetry software tools, SfM also allows for reliable processing of a large number of images in rather irregular image acquisition schemes (Snavely et al., 2008) and realises a much higher degree of process automation. Thus, one of the main differences between usual photogrammetric workflow and SfM is the emphasis on either accuracy or automation, with SfM focusing on the latter (Pierrot-Deseilligny and Clery, 2011).

Another deviation between both 3-D reconstruction methods is the consideration of GCPs (James and Robson, 2014a; Eltner and Schneider, 2015). Photogrammetry performs BBA either one-staged, considering GCPs within the BBA, or two-staged, performing geo-referencing after a relative image network configuration has been estimated (Kraus, 2007). In contrast, SfM is solely performed in the manner of a two-staged BBA concentrating on the relative orientation in an arbitrary coordinate system. Thus, absolute orientation has to be conducted separately with a seven parameter 3-D-Helmerttransformation, i.e. three shifts, three rotations and one scale. This can be done with the freeware tool sfm-georef that also gives accuracy information (James and Robson, 2012). Using GCPs has been proven to be relevant for specific geometric image network configurations, as parallel-axes image orientations usual for UAV data, because adverse error propagation can occur due to unfavourable parameter correlation, e.g. resulting in the non-linear error of a DEM dome (Wu, 2014; James and Robson, 2014a; Eltner and Schneider, 2015). Within a one-staged BBA these errors are avoided because during the adjustment calculation additional information from GCPs is employed, which is not possible, when relative and absolute orientation are not conducted in one stage.

The resulting oriented image block allows for a subsequent dense matching, measuring many more surface points through spatial intersection to generate a DSM with very high resolution. Recent developments in dense matching allow for resolving object coordinates for almost every pixel. To estimate 3-D coordinates, pixel values are either

ESURFD
3, 1445–1508, 2015

compared in image-space in the case of stereo-matching, considering two images, or in the object space in the case of MVS-matching, considering more than two images (Remondino et al., 2014). Furthermore, local or global optimisation functions (Brown et al., 2003) are considered, e.g. to handle ambiguities and occlusion effects between compared pixels (e.g. Pears et al., 2012). To optimise the pixel match, (semi-)global constraints consider the entire image or image scan-lines (usually utilised for stereo-matching, Remondino et al., 2014; e.g. semi-global matching (SGM) after Hirschmüller, 2011), whereas local constraints consider a small area in direct vicinity of the pixel of interest (usually utilised for MVS-matching, Remondino et al., 2014).

SfM photogrammetry software packages are available partially as freeware or even open-source (e.g. Visual SfM, Bundler or APERO). Most of the packages comprise SfM techniques in order to derive 3-D reconstructions from any collection of unordered photographs, without the need of providing camera calibration parameters and high accuracy ground control points. As a consequence, no in-depth knowledge in photogrammetric image processing is required in order to reconstruct geometries from overlapping image collections (James and Robson, 2012; Westoby et al., 2012; Fonstad et al., 2013). But now, also many photogrammetric tools utilise abilities from SfM to derive initial estimates automatically (i.e. automation) and then perform photogrammetric BBA with the possibility to set weights of parameters for accurate reconstruction performance (i.e. accuracy). In this review studies are considered, which either use straight SfM tools from computer vision or photogrammetric tools implementing SfM algorithms that entail no need for initial estimates in any regard.

3 Application of SfM photogrammetry in geosciences

A survey of 61 scientific papers published between 2012 and 2015 revealed a wide range of applications of SfM photogrammetry for geo-scientific analysis (see Table A1). The previously described advantages of the method introduce a new group of users, leading to a variety of new studies in geomorphic surface reconstruction and analy-

ESURFD
3, 1445–1508, 2015

sis. Different disciplines started to use SfM algorithms more or less simultaneously. It should be noted that common scientific journals, databases and standard online searches do not guarantee complete coverage of all studies about SfM photogrammetry in geosciences. Nevertheless, various disciplines, locations and approaches from all continents are contained in this review (Fig. 2).

A list of all topics reviewed in this manuscript according to their year of appearance is shown in Table 2. It is important to note that most subjects are not strictly separable from each other: a heavy flash flood event will likely trigger heavy damage by soil erosion or upstream slope failures. Thus, corresponding studies are arranged in regard to their major focus. The topic soil science comprises studies of soil erosion as well as soil micro-topography.

To put research hot spots in perspective it should be taken into account, that the number of publications from each discipline is not only dependent on the applicability of the method in that specific field of research. To a greater degree it is closely linked to the overall number of studies, which in the end can probably be broken down to the actual amount of researchers in that branch of science. Relative figures revealing the relation between SfM photogrammetry oriented studies to all studies of a given field of research would be desirable but are beyond the scope of this review.

3.1 Soil science

An identification of convergent research topics of SfM photogrammetry in geosciences revealed a distinct focus on erosional processes, especially in soil erosion (11 studies). Gullies, as often unvegetated and morphologically complex features of soil erosion, are predestined to serve as a research object (6 studies) to evaluate SfM photogrammetry performance. One of the first works on SfM in geosciences from 2012 compared established 2-D and 3-D field methods for assessing gully erosion (e.g. LiDAR, profile meter, total station) to SfM photogrammetry with regard to costs, accuracy and effectiveness revealing the superiority of SfM photogrammetry (Castillo et al., 2012). Also for a gully system, Stöcker et al. (2015) demonstrated the flexibility of SfM photogramme-

ESURFD
3, 1445–1508, 2015

try by combining independently captured terrestrial images with reconstructed surface models from UAV images to fill data gaps and achieve a comprehensive 3-D model. Another advantage of SfM photogrammetry – surface measurement of large coverage with very high resolution – allowed for a new assessment of plot based soil erosion analysis (Eltner et al., 2015).

Another 6 studies tackle the 3-D reconstruction of soil micro-topography by producing very dense point clouds or DEMs. This data further serves to assess pros and cons of SfM photogrammetry, e.g. with regard to the doming effect (Eltner and Schneider, 2015), to detect small-scale erosion features (Nouwakpo et al., 2014) or as input parameter for erosion modelling (Kaiser et al., 2015).

3.2 Volcanology

Volcanology is a pioneering area of SfM photogrammetry research in geosciences because 3 out of 6 studies in 2012 included volcanic research sites. James and Robson (2012) acquired information on volcanic dome volume and structural variability prior to an explosion from multi-temporal imagery taken from a light airplane. Brotheland et al. (2015) also surveyed volcanic dome dynamics with airborne imagery, but at larger scale for a resurgent dome. Another interesting work by Bretar et al. (2013) successfully reveals roughness differences in volcanic surfaces from lapilli deposits to slabby pahoehoe lava.

3.3 Glaciology

Glaciology and associated moraines are examined in 7 publications. Rippin et al. (2015) present a fascinating UAV-based work on supra-glacial runoff networks, comparing the drainage system to surface roughness and surface reflectance measurements and detecting linkages between all three. In several UAV campaigns Immerzeel et al. (2014) detected limited mass losses and low surface velocities but high local variations of melt rates that are linked to supra-glacial ponds and ice cliffs.

ESURFD
3, 1445–1508, 2015

3.4 Mass movements

Mass movements were monitored by Stumpf et al. (2014) at a landslide. During several measuring campaigns the accuracy of two 3-D reconstruction tools were tested and compared to LiDAR data. Furthermore, seasonal dynamics of the landslide body and different processes, like lobes and rock fall, could be separated.

3.5 Fluvial morphology

Channel networks in floodplains were surveyed by Prosdocimi et al. (2015) in order to analyse eroded channels banks and to quantify the transported material. Besides classic DSLR cameras, evaluation of an iPhone camera revealed sufficient accuracy, so that in near future also farmers are able to carry out post event documentation of damage. An interesting large scale riverscape assessment is presented by Dietrich (2016), who carried out a helicopter based data acquisition of a 32 km river segment. A small helicopter proves to close the gap between unmanned platforms and commercial aerial photography from airplanes.

3.6 Coastal morphology

In the pioneering article by Westoby et al. (2012) several morphological features of contrasting landscapes where chosen to test the capabilities of SfM; one of them being a coastal cliff of roughly 80 m height. Up to 90 000 points m^{-2} enabled the identification of bedrock faulting. Ružić et al. (2014) produced surface models of coastal cliffs that have been retreating up to 5 m since the 1960s to test the abilities of SfM photogrammetry in undercuts and complex morphologies.

3.7 Others

In addition to the prevalent fields of attention also more exotic research is carried out unveiling unexpected possibilities for SfM photogrammetry. Besides the benefit

ESURFD
3, 1445–1508, 2015

for the specific research itself, these branches are important as they either explore new frontiers in geomorphometry or demonstrate the versatility of the method. Lucieer et al. (2014) analyse artic moss beds and their health conditions by using high-resolution surface topography (2 cm DEM) to simulate water availability from snow melt. Leon et al. (2015) acquired underwater imagery of a coral reef to produce a DEM with a resolution of 1 mm for roughness estimation. Genchi et al. (2015) used UAV-image data of an urban cliff structure to identify bio erosion features and found a pattern in preferential locations.

The re-consideration of historical aerial images is another interesting opportunity arising from the new algorithmic image matching developments that allow for new DEM resolutions and thus possible new insights into landscape evolution (Gomez et al., 2015). Also accounting for the temporal scale, completely new insights can be achieved by time-lapse analysis, already demonstrated by James and Robson (2014b), who monitored a lava flow at minute intervals.

4 Non-commercial tools for SfM photogrammetry and data post-processing

Initiatives based on non-commercial software have played a significant role in the development of SfM photogrammetry approaches, either open-source, meaning the source code is available with a license for modification and distribution, or freely-available, meaning the tool is free to use but no source code is provided (Table B1). The pioneer works by Snavely et al. (2006, 2008) and Furukawa and Ponce (2010) as well as Furukawa et al. (2010) provided the basis to implement one of the first open-source workflows for free SfM photogrammetry combining Bundler and PMVS2/CMVS as in SfMToolkit (Astre, 2015). By 2007, the MicMac project, which is open-source software originally developed for aerial image matching, became available to the public and later evolved to a comprehensive SfM photogrammetry pipeline with further tools such as APERO (Pierrot-Deseilligny and Clery, 2011).

ESURFD
3, 1445–1508, 2015

Further contributors put their efforts in offering freely-available solutions based on Graphical User Interfaces (GUI) for image-based 3-D reconstruction (VisualSfM by Wu, 2013) and geo-referencing (sfm_georef by James and Robson, 2012). The need for editing large point-cloud entities from 3-D reconstruction led to the development of open-source specific tools such as Meshlab (Cignoni et al., 2008) or CloudCompare (Girardeau-Montaut, 2015), also implementing GUIs. Sf3M (Castillo et al., 2015) exploits VisualSfM and sfm_georef and additional CloudCompare command-line capacities for image-based surface reconstruction and subsequent point cloud editing within one GUI tool. Overall, non-commercial applications have provided to date a wide range of SfM photogrammetry related solutions that are constantly being improved on the basis of collaborative efforts.

A variety of tools of SfM photogrammetry (at least 10 different) are used within the differing studies of this review (Fig. 3). Agisoft PhotoScan is by far the most employed software, which is probably due to its ease of use. However, this software is commercial and works after the black box principle, which is in contrast to the second most popular tools Bundler in combination with PMVS or CMVS. The tool APERO in combination with MicMac focuses on accuracy instead of automation (Pierrot-Deseilligny and Clery, 2011), which is different to the former two. The high degree of possible user-software interaction that can be very advantageous to adopt the 3-D reconstruction to each specific case study might also be its drawback because further knowledge into the method is required. Only a few studies have used the software in geo-scientific investigations (Bretar et al., 2013; Stumpf et al., 2014; Ouédraogo et al., 2014; Stöcker et al., 2015; Eltner and Schneider, 2015).

5 Performance of SfM photogrammetry in geo-scientific applications

It is important to have method independent references to evaluate 3-D reconstruction tools confidently. This time, 39 studies are investigated (Table A1), where a reference has been setup, either area based (e.g. TLS) or point based (e.g. RTK GPS points).

ESURFD
3, 1445–1508, 2015

Because not all studies perform accuracy assessment with independent references, the number of studies is in contrast to the number of 61 studies that were reviewed in regard to applications in Sect. 3.

5.1 Error terms

A definite designation of error parameters is performed prior to comparing the studies to avoid using ambiguous terms. There is a difference between local surface quality and more systematic errors, i.e. due to referencing and project geometry (James and Robson, 2012). Specifically, error can be assessed in regard to accuracy and precision.

Accuracy defines the closeness of the measurement to the true surface and usually implies systematic errors, which can be displayed by the mean error value. For the evaluation of two DEMs, the iterative closest point (ICP) algorithm can improve the accuracy significantly if a systematic linear error (e.g. shifts, tilts or scale variations) is given, as demonstrated by Micheletti et al. (2014).

Precision defines the repeatability of the measurement, e.g. it indicates how rough an actual planar surface is represented. Precision usually comprises random errors and is measured with the standard deviation or RMSE. However, precision is not independent from systematic errors. In this study, focus lies on precision which also might be influenced by systematic errors and thus the general term "measured error" is used.

Registration residuals of GCPs resulting from BBA allow for a first error assessment. But it is not sufficient as exclusive error measure due to potential deviations between the true surface and the calculated statistical and geometric model, which are not detectable with the GCP error vectors alone because BBA is optimised to minimise the error at these positions. However, if BBA has been performed two-staged (i.e. SfM and referencing calculated separately), the residual vector provides reliable quality information because registration points are not integrated into model estimation.

Further error evaluation in this study is performed with reference measurements. Thereby, errors due the performance of the method itself and errors due to the method of quality assessment have to be distinguished.

ESURFD
3, 1445–1508, 2015

5.2 Error sources of image-based 3-D reconstruction

The error of 3-D reconstruction is influenced by many factors: scale/distance, camera calibration, image network geometry, image matching performance, surface texture and lighting conditions, and GCP characteristics, which are examined in detail in this section. The statistical analysis of the achieved accuracies of the reviewed studies is performed with the Python Data Analysis Library (panda). If several errors were measured with the same setup, e.g. in the case of multi-temporal assessments, the average value is applied. Furthermore, outliers that complicated data visualisation, were neglected within the concerning plots. This concerned the study of Dietrich (2016) due to a large scale, the study of Snapir et al. (2014) due to a high reference accuracy and Frankl et al. (2015) due to a high measured error.

5.2.1 Scale and sensor to surface distance

SfM photogrammetry contains the advantage to be useable at almost any scale. Thus, in the reviewed studies the method is applied at a large range of scales (Fig. 4), reaching from 10 cm for volcanic bombs (Favalli et al., 2012; James and Robson, 2012) up to 10 km for a river reach (Dietrich, 2016). Median scale amounts about 100 m. SfM photogrammetry reveals a scale dependent practicability (Smith and Vericat, 2015) if case study specific tolerable errors are considered, e.g. for multi-temporal assessments. For instance, at plot and hillslope scale 3-D reconstruction is a very sufficient method for soil erosion studies, even outperforming TLS (Nouwakpo et al., 2015; Eltner et al., 2015; Smith and Vericat, 2015). The method should be most useful in small scale study reaches (Fonstad et al., 2013), whereas error behaviour is not as advantageous for larger scales, i.e. catchments (Smith and Vericat, 2015).

Besides scale, observation of the distance between sensor and surface is important for image-based reconstructed DEM error, also because scale and distance interrelate. The comparison of the reviewed studies indicates that with an increase of distance the measured error decreases, which is not unexpected (Fig. 5, circles). However, there

ESURFD
3, 1445–1508, 2015

is no linear trend detectable. Therefore, a uniform error ratio (or relative error), which is calculated by dividing distance with measured error, is not assignable. The error ratio itself displays a large range from 15 to 4000 with a median of 400, thus revealing a rather low error potential (Fig. 5, triangles). Very high ratios are solely observable for very close-range applications and at large distances. A general increase of the error ratio with distance is observable (Fig. 5, triangles). The indication that cm-accurate measurements are realisable at distances below 200 m (Stumpf et al., 2014) can be confirmed by Fig. 5 because most deviations are below 10 cm until that range. Overall, absolute error values are low at close ranges, whereas the error ratio is higher at larger distances.

5.2.2 Camera calibration

SfM photogrammetry allows for straight forward handling of camera options due to integrated self-calibration, but knowledge about some basic parameters is necessary to avoid unwanted error propagation into the final DEM from insufficiently estimated camera models. The autofocus as well as automatic camera stabilisation options should be deactivated if a pre-calibrated camera model is used or one camera model is estimated for the entire image block because changes in the interior camera geometry due to camera movement cannot be captured with these settings. The estimation of a single camera model for one image block is usually preferable, if a single camera has been used, whose interior geometry is temporary stable, to avoid over parameterisation (Pierrot-Deseilligny and Clery, 2011). Thus, if zoom lenses are moved a lot during data acquisition, they should be avoided due to their instable geometry (Shortis et al., 2006; Sanz-Ablanedo et al., 2010) that impedes usage of pre-calibrated fixed or single camera models. A good compromise between camera stability, sensor size and equipment weight, which is more relevant for UAV applications, are achieved by compact system cameras (Eltner and Schneider, 2015). However, solely three studies utilize compact system cameras in the reviewed studies (Tonkin et al., 2014; Eltner and Schneider, 2015; Eltner et al., 2015).

ESURFD
3, 1445–1508, 2015

Along with camera settings, the complexity in regard to the considered parameters of the defined camera model within the 3-D reconstruction tool is relevant, i.e. to avoid DEM domes as a consequence of insufficient image distortion estimation (James and Robson, 2014a; Eltner and Schneider, 2015). Also, Stumpf et al. (2014) detect worse distortion correction with a basic SfM tool, considering a simple camera model, compared to more complex software, integrating a variety of camera models. Camera calibration is a key element for high DEM quality, which is extensively considered in photogrammetric software, whereas simpler models that solely estimate principle distance and radial distortion are usually implemented in the SfM tools originating from computer vision (Eltner and Schneider, 2015; James and Robson, 2012; Pierrot-Deseilligny and Clery, 2011). Figure 6 also demonstrates that at same distances more extensive 3-D reconstruction tools, implementing more complex camera models and several GCP integration possibilities (e.g. APERO, Pix4-D, Agisoft PhotoScan) produce lower errors compared to tools considering basic camera models and no GCPs (e.g. Visual SfM, Bundler).

5.2.3 Image resolution

Image resolution is another factor influencing the final DEM quality. Especially, the absolute pixel size needs to be accounted for due to its relevance for the signal-to-noise ratio (SNR) because the larger the pixel the higher the amount of light that can be captured and hence a more distinct signal is measured. Resolution alone by means of pixel number gives no information about the actual metric sensor size. A large sensor with large pixels and a large amount of pixels provides better image quality due to reduced image noise than a small sensor with small pixels but the same amount of pixels. Thus, high image resolution defined by large pixel numbers and pixel sizes resolves in sufficient quality of images and thus DEMs (Micheletti et al., 2014; Eltner and Schneider, 2015).

However, in this study the reviewed investigations indicate no obvious influence of the pixel size at the DEM quality (Fig. 7). Mostly, cameras with middle sized sensors

ESURFD
3, 1445–1508, 2015

and corresponding pixel sizes around 5 µm are used. In studies with pixel sizes larger 7 µm an error ratio above 500 is observable. But else a large range of error at different pixel sizes can be seen, which might be due to other error influences superimposing the impact of pixel size. Thus, more data is needed for significant conclusions.

To speed up processing, down-sampling of images is often performed causing interpolation of pixels and thus the reduction of image information, which can be the cause for underestimation of high relief changes, e.g., observed by Smith and Vericat (2015) or Nouwakpo et al. (2015). Interestingly, Prosdocimi et al. (2015) reveal that lower errors are possible with decreasing resolution due to an increase of error smoothing. Nevertheless, image data collection in the field should be done at highest realisable resolution and highest SNR to fully keep control over subsequent data processing, i.e. data smoothing should be performed under self-determined conditions at the desktop, which is especially important for studies of rough surfaces to allow for probate error statistics (e.g. Brasington et al., 2012).

5.2.4 Image network geometry

In regard to the geometry of the image network several parameters are important: number of images, image overlap, obliqueness, and convergence.

At least three images need to capture the area of interest, but for redundancy to decrease DEM error higher numbers are preferred (James and Robson, 2012). For instance, Piermattei et al. (2015) detect better qualities for a higher amount of images. However, the increase of images does not linearly increase the accuracy (Micheletti et al., 2014), and may ultimately lead to unnecessary increase in computation time. Generally, image number should be chosen depending on the size and complexity of the study reach (James and Robson, 2012); as high as possible but still keeping in mind acceptable processing time. The reviewed studies do not allow for distinct relation conclusions between 3-D reconstruction performance and image number because the DEM error also interferes with other parameters, e.g. such as object complexity, image overlap or image convergence (Fig. 8).

ESURFD
3, 1445–1508, 2015

High image overlap is relevant to finding homologous points within many images that cover the entire image space. Stumpf et al. (2014) show that higher overlap resolves in better results, even though ground sampling distance decreases due to a smaller focal length. Wide angle lenses, whose radial distortion is within the limits, should be chosen for data acquisition.

The reviewed studies reveal a large variety of applicable perspectives for DEM generation (Table 3). Most applications use images captured from the ground, which is the most flexible implementation of the SfM photogrammetry method. In regard to terrestrial or aerial perspective, Smith and Vericat (2015) state that aerial images should be preferred if plots reach sizes larger 100 m because at these distances obliqueness of images becomes too adverse. Stumpf et al. (2014) even mention a distinct value of the incidence angle of 30° to the captured surface above which data quality decreases significantly.

Furthermore, image network geometry has to be considered separately for convergent acquisitions schemes, common for terrestrial data collection, and for parallel-axes acquisition schemes, common for aerial data collection. The parallel-axes image configuration results in unfavourable error propagation due to unfavourable parameter correlation, which inherits the separation between DEM shape and radial distortion (James and Robson, 2014a; Wu, 2014) resulting in a dome error that needs either GCP implementation or a well estimated camera model for error mitigation (James and Robson, 2014a; Eltner and Schneider, 2015). However, GCP accuracy has to be sufficient or else the weight of GCP information during BBA is too low to avoid unfavourable correlations, as shown by Dietrich (2016), where DEM dome error within a river reach could not be diminished even though GCPs were implemented into 3-D reconstruction. If convergent images are utilised, the angle of convergence is important because the higher the angle the better the geometry and thus accuracy because sufficient image overlap with larger bases between images is possible and thus less difficulties due to glancing ray intersections arise. But simultaneously, convergence should not be so

ESURFD
3, 1445–1508, 2015

high that the imaged scene becomes too contradictory for successful image matching (Pierrot-Deseilligny and Clery, 2012; Stöcker et al., 2015).

5.2.5 Accuracy and distribution of homologues image points

The quality of DEMs reconstructed from overlapping images depends significantly on the image-matching performance (Grün, 2012). Image content and type, which cannot be enhanced substantially, are the primary factors controlling the success of image-matching (Grün, 2012). Image-matching is important for reconstruction of the image network geometry as well as the subsequent dense-matching.

On the one hand, it is relevant to find good initial matches (e.g. SIFT features are not as precise as least square matches with $\frac{1}{10}$ pixel size accuracies; Grün, 2012) to perform reliable 3-D reconstruction and thus retrieve an accurate sparse point cloud because MVS approaches for dense matching as well as optimization procedures for model refinement rely on this first point cloud. Thus, immanent errors will propagate along the different stages of SfM photogrammetry.

On the other hand, more obviously image-matching performance is important for dense reconstruction, when 3-D information is calculated for almost every pixel. The accuracy of intersection during dense matching depends on the accuracy of the estimated camera orientations (Remondino et al., 2014). If the quality of the DEM is the primary focus, which is usually not the case for SfM algorithms originating from computer vision, the task of image-matching is still difficult (Grün, 2012). Nevertheless, newer approaches are emerging, though, which still need evaluation in respect of accuracy and reliability (Remondino et al., 2014). An internal quality control for image-matching is important for DEM assessment (Grün, 2012), but are mostly absent in tools for image-based 3-D reconstruction.

So far, many studies exist, which evaluate the quality of 3-D reconstruction in geoscientific applications. Nevertheless, considerations of dense-matching performance are still missing, especially in regard of rough topographies (Eltner and Schneider, 2015).

ESURFD
3, 1445–1508, 2015

5.2.6 Surface texture

Texture and contrast of the area of interest is significant to identify suitable homologues image points. Low textured and contrasted surfaces result in a distinct decrease of image features, i.e. snow covered glaciers (Gómez-Gutiérrez et al., 2014a) or sandy beaches (Mancini et al., 2013). Furthermore, vegetation cover complicates image matching performance due to its highly variable appearance from differing viewing angles (e.g. Castillo et al., 2012; Eltner et al., 2015) and possible movements during wind. Thus, in this study, if possible, only studies of bare surfaces are reviewed for error assessment.

5.2.7 Illumination condition

Over- and under-exposure of images is another cause of error in the reconstructed point cloud, which cannot be significantly improved by utilising HDR images (Gómez-Gutiérrez et al., 2015). Well illuminated surfaces result in a high number of detected image features, which is demonstrated for coastal boulders under varying light conditions by Gienko and Terry (2014). Furthermore, Gómez-Gutiérrez et al. (2014a) highlight the unfavourable influence of shadows because highest errors are measured in these regions; interestingly, these authors calculate the optimal time for image acquisition from the first DEM for multi-temporal data acquisition. Generally, overcast but bright days are most suitable for image capture to avoid strong shadows or glared surfaces (James and Robson, 2012).

5.2.8 GCP accuracy and distribution

GCPs are important inputs for data referencing and scaling. Photogrammetry always stresses the weight of good ground control for accurate DEM calculation, especially if one-staged BBA is performed. In the common SfM workflow integration of GCPs is less demanding because they are only needed to transform the 3-D-model from the arbi-

ESURFD
3, 1445–1508, 2015

trary coordinate system, which is comparable to the photogrammetric two-staged BBA processing. A minimum of three GCPs are necessary to account for model rotation, translation and scale. However, GCP redundancy, thus more points, has been shown to be preferable to increase accuracy (James and Robson, 2012). A high number of GCPs further ensures the consideration of checkpoints not included for the referencing, which are used as independent quality measure of the final DEM. More complex 3-D reconstruction tools either expand the original 3-D-Helmert-transformation by secondary refinement of the estimated interior and exterior camera geometry to account for non-linear errors (e.g. Agisoft PhotoScan) or integrate the ground control into the BBA (e.g. APERO).

Natural features over stable areas, which are explicitly identifiable, are an alternative for GCP distributions, although they usually lack strong contrast (as opposed to artificial GCPs) that would allow for automatic identification and sub-pixel accurate measurement (e.g. Eltner et al., 2013). Nevertheless, they can be suitable for multi-temporal change detection applications, where installation of artificial GCPs might not be possible or necessary as in some cases relative accuracy is preferred over absolute performance (e.g. observation of landslide movements, Turner et al., 2015).

GCP distribution needs to be even and adapted to the terrain resulting in more GCPs in areas with large changes in relief (Harwin and Lucieer, 2012) to cover different terrain types. Harwin and Lucieer (2012) state an optimal GCP distance between $\frac{1}{5}$ and $\frac{1}{10}$ of object distance for UAV applications. Furthermore, the GCPs should be distributed at the edge or outside the study area (James and Robson, 2012) to enclose the area of interest, because if the study reach is extended outside the GCP area, a significant increase of error is observable in that region (Smith et al., 2014; Javernick et al., 2014; Rippin et al., 2015).

The measurement of GCPs can be performed either within the point cloud or the images, preferring the latter because identification of distinct points in 3-D point clouds of varying density can be less reliable (James and Robson, 2012; Harwin and Lucieer, 2012) compared to sub-pixel measurement in 2-D images, where accuracy of

ESURFD
3, 1445–1508, 2015

GCP identification basically depends on image quality. Figure 5 illustrates that only few studies measured GCPs in point clouds producing higher errors compared to other applications at the same distance.

5.3 Errors due to accuracy/precision assessment technique

5.3.1 Reference of superior accuracy

It is difficult to find a suitable reference for error assessment of SfM photogrammetry in geo-scientific or geomorphologic applications due to the usually complex and rough nature of the studied surfaces. So far, either point based or area based measurements are carried out. On the one hand, point based methods (e.g. RTK GPS or total station) ensure superior accuracy but lack sufficient area coverage for precision statements of local deviations; on the other hand, area based (e.g. TLS) estimations are used, which provide enough data density but can lack of sufficient accuracy (Eltner and Schneider, 2015). Roughness is the least constrained error within point clouds (Lague et al., 2013) independent from the observation method. Thus, it is difficult to distinguish between method noises and actual signal of method differences, especially at scales where the reference method reaches its performance limit. For instance Tonkin et al. (2014) indicate that the quality of total station points is not necessarily superior on steep terrain.

Generally, 75 % of the investigations reveal a measured error that is lower than 20 times the reference error. But the median shows that superior accuracy assessment is actually significantly poorer; the measured error (measured error divided by reference accuracy) is merely twice the reference error (Fig. 4). The reviewed studies further indicate that the superior accuracy of the reference seems scale dependent (Fig. 9). In shorter distances (below 50 m) most references reveal accuracies that are lower than one magnitude superiority to the measured error. However, alternative reference methods are yet absent. Solely, for applications in further distances the references are sufficient. These findings are relevant for the interpretation of the error ratio because low ratios at small scale reaches might be due to the low performance of the reference

ESURFD
3, 1445–1508, 2015

rather than the actual 3-D reconstruction quality but due to the reference noise lower errors are not detectable. Low error ratios are measured where the superior accuracy is also low (distance 5–50 m) and large ratios are given at distance where superior accuracy increases as well.

5.3.2 Type of deviation measurement

The reviewed studies use different approaches to measure the distance between the reference and the 3-D reconstructed DEM. Comparison are either performed in 2.5-D (raster) or real 3-D (point cloud). Lague et al. (2013) highlight that the application of raster inherits the disadvantage of data interpolation, especially relevant for rough surfaces or complex areas (e.g. undercuts as demonstrated for gullies by Frankl et al., 2015). In this context it is important to note that lower errors are measured for point-to-point distances rather than raster differencing (Smith and Vericat, 2015; Gómez-Guiérrez et al., 2014b).

Furthermore, within 3-D evaluation different methods for deviation measurement exist. The point-to-point comparison is solely suitable for a preliminary error assessment because this method is prone to outliers and differing point densities. By point cloud interpolation alone (point-to-mesh), this issue is not solvable because there are still problems at very rough surfaces (Lague et al., 2013). Different solutions have been proposed: On the one hand, Abellan et al. (2009) proposed averaging the point cloud difference along the spatial dimension, which can also be extended to 4-D (x, y, z, time; Kromer et al., 2015). On the other hand, Lague et al. (2013) proposed the M3C2 algorithm for point cloud comparison that considers the local roughness and further computes the statistical significance of detected changes. Stumpf et al. (2014) and Gómez-Gutiérrez et al. (2015) illustrated lower error measurements with M3C2 compared to point-to-point or point-to-mesh. Furthermore, Kromer et al. (2015) showed how the 4-D filtering, when its implementation is feasible, allows to considerably increase the level of detection compared to M3C2.

ESURFD
3, 1445–1508, 2015

5.4 Standardised error assessment

To compare the achieved accuracies and precisions of different studies a standardised error assessment is necessary. In this review, besides actual measured error comparison, theoretical errors for the convergent image configuration are calculated (Eq. 1, Fig. 10) to compare if applications in the field achieved photogrammetric accuracy (Luhman et al., 2014). It is not possible to evaluate the theoretical error for parallel-axes case studies because information about the distance between subsequent images is mostly missing. However, Eltner and Schneider (2015) and Eltner et al. (2015) compare their results to parallel-axes theoretical error and could demonstrate that for soil surface measurement from low flying heights at least photogrammetric accuracy is possible.

$$\sigma_c = \frac{q\overline{D}}{\sqrt{k}d}\sigma_i \quad (1)$$

Being:

σ_c coordinate error,

q strength of image configuration (set to 1; according to James and Robson, 2012)

k number of images (set to 3; according to James and Robson, 2012)

D mean distance object-target,

d principle distance,

σ_i error image measurement (0.29 due to quantisation noise)

The results from James and Robson (2012), which show a less reliable performance of SfM than expected from photogrammetric estimation, can be confirmed by the reviewed studies. Image-based 3-D reconstruction, considering SfM workflows, perform

ESURFD
3, 1445–1508, 2015

poorer than the theoretical error (Fig. 9). The measured error is always higher and on average 90 times worse than the theoretical error. Even for the smallest ratio the actual error is 6 times higher. Furthermore, it seems that with increasing distance theoretical and measured errors converge slightly.

As demonstrated, diverse factors influence SfM photogrammetry performance and subsequent DEM error with different sensitivity. Generally, accurate and extensive data acquisition is necessary to minimise error significantly (Javernick et al., 2014). Independent reference sources, such as TLS, are not replaceable (James and Robson, 2012) due to their differing error properties (i.e. error reliability) compared to image-matching (Grün, 2012). Synergetic effects of SfM and classical photogrammetry should be used, i.e. benefiting from the high automation of SfM to retrieve initial estimates without any prior knowledge about the image scene and acquisition configuration and adjacent reducing error by approved photogrammetric approaches, which are optimised for high accuracies.

The reviewed studies indicate the necessity of a standardised protocol for error assessment because the variety of studies inherit a variety of scales worked at, software used, GCP types measured, deviation measures applied, image network configurations implemented, cameras and platforms operated and reference utilised, making it very difficult to compare results with consistency. Relevant parameters for a standard protocol are suggested in Table 4.

6 Perspectives and limitations

SfM photogrammetry has allowed capturing massive three-dimensional datasets by non-specialists during the last five years, and it is highly expected that this technique will evolve during the forthcoming years. Current studies are focusing into capturing the terrain's geometry with high precision, but several opportunities for using point clouds to improve our understanding, modelling and prediction of different earth surface processes still remain unexplored. In return, some technical and operational aspects are

ESURFD
3, 1445–1508, 2015

still limiting our ability to acquire datasets over naturally complex outcrops. Some issues that need to be addressed include the progressive degradation of the data quality at longer distances, the effect of a limited depth of field on the point cloud quality, the occurrence of biases and occlusions that can strongly influence the quality of the acquired datasets, the use of super-macro and super-zoom lenses for investigating unexplored natural phenomena, between others. Eventually, SfM photogrammetry technique may become a mainstream procedure during the next decade, perspectives include efforts in cross-disciplinarity, process automatisation, data and code sharing, real time data acquisition and processing, unlocking the archives, etc., as follows:

6.1 Cross-disciplinarity

A great potential relies on adapting three dimensional methods originally developed for the treatment of 3-D LiDAR data to investigate natural phenomena through SfM photogrammetry techniques. Applications, dating back from the last decade, must be integrated into SfM photogrammetry post-processing; examples include: geomorphological investigations in high mountain areas (Milan et al., 2007), geological mapping (Buckley et al., 2008; Franceschi et al., 2009), soil erosion studies (Eltner and Baumgart, 2015), investigation of fluvial systems (Heritage and Hetherington, 2007; Cavalli et al., 2008; Brasington et al., 2012), and mass wasting phenomena (Lim et al., 2005; Oppikofer et al., 2009; Abellan et al., 2010).

More specifically, several data treatment techniques have been developed during the last decade for different situations, which will need to be known, adapted and enriched by the growing SfM photogrammetry community; examples include: automatic lithological segmentation according to the intensity signature (Humair et al., 2015), integration of ground based LiDAR with thermal/hyperspectral imaging for lithological discrimination (Kääb, 2008; Hartzell et al., 2014), extraction of the structural settings on a given outcrop (Jaboyedoff et al., 2007; Sturzenegger and Stead, 2009; Gigli and Casagli, 2011; Riquelme et al., 2014), automatic extraction of surface roughness (Poropat, 2009) of the discontinuity spacing/persistence/waviness (Fekete et al., 2010;

ESURFD
3, 1445–1508, 2015

Khoshelham et al., 2011; Pollyea and Fairley, 2011), bi- and three-dimensional tracking of mass movements (Teza et al., 2007; Monserrat and Crosetto, 2008), investigation of progressive failures (Royan et al., 2015; Kromer et al., 2015), and usage of mobile systems (Lato et al., 2009; Michoud et al., 2015).

6.2 Process-automatisation

Handling huge databases is an important issue and although fully automatic techniques may not be necessary, a series of tedious and manual processes are still required for data treatment. The development of open-source software for handling huge 3-D datasets such as CloudCompare (Girardeau-Montaut, 2015) has considerably boosted geomorphological studies using 3-D point clouds. Nevertheless, sharing the source code of specific applications for investigating earth surface processes is still scarce.

6.3 Data and code sharing

Open data in geomorphological studies using point clouds is also needed. Again, a series of databases exist for LiDAR datasets (openTopography.org, rockbench.com, 3-D-landslide.com). But up to the knowledge of these authors, there is no specific Git-Hub cluster or website dedicated to the maintaining and development of open-access software in geosciences.

6.4 Unlocking the archive

The appraisal of digital photography and the exponential increase of data storage capabilities have enabled the massive archive of optical images around the world. Accessing to such quantity of information could provide unexpected opportunities for the four dimensional research of geomorphological processes using SfM photogrammetry workflows. Except for some open repositories (e.g. Flickr, Google street view) the possibility to access the massive optical data is still scarce. In addition, accessing to such databases may become a challenging task due to data interchangeability issues.

ESURFD
3, 1445–1508, 2015

A considerable effort may be necessary for creating such database with homogeneous data formats and descriptors (type of phenomenon, temporal resolution, pixel size, accuracy, distance to object, existence of GCPs, etc.) during the forthcoming years.

A first valuable approach to use data from online imagery was presented by Martin-Brualla et al. (2015), who pave the way for further research in a new field of 3-D surface analysis (i.e. time-lapse). Other possible applications might unlock the archive of airborne, helicopter-based or terrestrial imaginary, ranging from the estimation of coastal retreat rates, the observation of the evolution of natural hazards to the monitoring of glacier fronts, and further.

6.5 Real time data acquisition

Rapid developments in automatisation (soft- and hardware wise) allow for in situ data acquisition and its immediate transfer to processing and analysing institutions. Thus, extreme events are recognisable during their occurrence and authorities or rescue teams can be informed in real-time. In this context SfM photogrammetry could help to detect and quantify rapid volume changes of e.g. glacier fronts, pro-glacial lakes, rock failures and ephemeral rivers.

Furthermore, real-time crowd sourcing offers an entirely new dimension of data acquisition. Due to the high connectivity of the public through smartphones, various possibilities arise to share data (Johnson-Roberson et al., 2015). An already implemented example is real-time traffic information. Jackson and Magro (2015) name further options. Crowd sourced imagery can largely expand possibilities to 3-D information.

6.6 Time-lapse photography

A limited frequency of data acquisition increases the likelihood of superimposition and coalescence of geomorphological processes (Abellan et al., 2014). Since time-lapse SfM photogrammetry data acquisition has remained so far unexplored, a great prospect is expected on this topic during the coming years. One reason why time-lapse SfM

ESURFD
3, 1445–1508, 2015

photogrammetry remains rather untouched in geosciences lies in the complex nature of producing continuous data sets.

Besides the need for an adequate research site (frequent morphodynamic activity), other aspects have to be taken into account: an automatic camera setup is required with self-contained energy supply (either via insolation or wind), adequate storage and appropriate choice of viewing angles onto the area of interest. Furthermore, cameras need to comprise sufficient image overlap and have to be synchronised. Ground control is required and an automatic pipeline for large data treatment should be developed.

New algorithms are necessary to deal with massive point cloud databases. Thus, innovative four dimensional approaches have to be developed to take advantage of the information contained in real-time and/or time-lapse monitoring. Combining these datasets with climatic information can improve the modelling of geomorphological processes.

6.7 Automatic UAV surveying (no human controller)

Unmanned airborne vehicles already show a large degree of automatisation as they follow flight paths and acquire data autonomously. Human control is not required except for launching of the multi-copter or fixed wing system. Automatic landing is already provided by several systems. In near future a fully automatic UAV installation could comprise the following: repeated survey of an area of interest, landing and charging at a base station, data link for local storage or satellite based data transfer, and safety mechanism for preventing lift-off during inappropriate weather conditions. However, a large limitation for such realisation lies in legal restrictions because national authorities commonly request for visual contact to the UAV in case of failure. But in remote areas installation could already be allowed by regulation authorities.

ESURFD
3, 1445–1508, 2015

7 Conclusions

This review has shown the versatility and flexibility of the evolving method SfM photogrammetry, which is recapitulated in Fig. 11. Due to its beneficial qualities, a wide community of geoscientists starts to implement 3-D reconstruction based on images within a variety of studies. Summing up the publications, there are no considerable disadvantages mentioned (e.g. accuracy wise) compared to other methods that cannot be counteracted by placement of GCPs, camera calibration or a high image number. Frontiers in geomorphometry have been expanded once more, as limits of other surveying techniques such as restricted mobility, isolated area of application and high costs are overcome by the SfM photogrammetry. Its major advantages lie in easy-to-handle and cost-efficient digital cameras as well as non-commercial software solutions.

Performance analysis revealed the suitability of SfM photogrammetry at a large range of scales in regard to case study specific accuracy necessities. While research of the last years mainly focussed on testing the applicability of SfM photogrammetry in various geo-scientific applications, recent studies try to pave the way for future usages and develop new tools, setups or algorithms. However, different factors influencing final DEM quality still need to be addressed. This should be performed under strict experimental (laboratory) designs because complex morphologies, typical in earth surface observations, impede accuracy assessment due to missing superior reference. Thus, independent references and GCPs are still needed in SfM photogrammetry for reliable estimation of the quality of each 3-D reconstructed surface.

Fast and facile generation of DEM produces new challenges. The exploitation of the entire information of the SfM photogrammetry output (3-D point cloud or mesh instead of 2.5-D raster) will become a significant issue in future studies of high resolution topography (Passalacqua et al., 2015), which has to be even extended to 4-D when additionally considering time. Thus, especially comprehensive end user software needs further progress in these aspects.

ESURFD
3, 1445–1508, 2015

Nevertheless, SfM photogrammetry is already becoming an essential tool for digital surface mapping. It is employable in a fully automatic manner but individual adjustments can be conducted to account for each specific case study constrain and accuracy requirement in regard to the intended application. Due to the possibility of different degrees of process interaction, non-experts can utilise the method depending on their discretion.

Acknowledgements. The authors A. Eltner, A. Kaiser and F. Neugirg are funded by the German Research Foundation (DFG) (MA 2504/15-1, HA5740/3-1, SCHM1373/8-1). A. Abellan acknowledges founding by Univ. Lausanne and the RockRisk research project (BIA2013-42582-P).

References

Abellán, A., Jaboyedoff, M., Oppikofer, T., and Vilaplana, J. M.: Detection of millimetric deformation using a terrestrial laser scanner: experiment and application to a rockfall event, Nat. Hazards Earth Syst. Sci., 9, 365–372, doi:10.5194/nhess-9-365-2009, 2009.

Abellán, A., Calvet, J., Vilaplana, J. M., and Blanchard, J.: Detection and spatial prediction of rockfalls by means of terrestrial laser scanner monitoring, Geomorphology, 119, 162–171, doi:10.1016/j.geomorph.2010.03.016, 2010.

Abellán, A., Oppikofer, T., Jaboyedoff, M., Rosser, N. J., Lim, M., and Lato, M. J.: Terrestrial laser scanning of rock slope instabilities, Earth Surf. Proc. Land., 39, 80–97, doi:10.1002/esp.3493, 2014.

Ai, M., Hu, Q., Li, J., Wang, M., Yuan, H., and Wang, S.: A robust photogrammetric processing method of low-altitude UAV images, Remote Sensing, 7, 2302–2333, doi:10.3390/rs70302302, 2015.

Astre, H.: SfMtoolkit, available at: http://www.visual-experiments.com/demos/sfmtoolkit/, last access: 1 November 2015.

Bay, H., Ess, A., Tuytelaars, T., and Van Gool, L.: Speeded-Up Robust Features (SURF), Comput. Vis. Image Und., 110, 346–359, doi:10.1016/j.cviu.2007.09.014, 2008.

Bemis, S. P., Micklethwaite, S., Turner, D., James, M. R., Akciz, S., Thiele, S. T., and Bangash, H. A.: Ground-based and UAV-Based photogrammetry: a multi-scale, high-resolution

mapping tool for structural geology and paleoseismology, J. Struct. Geol., 69, 163–178, doi:10.1016/j.jsg.2014.10.007, 2014.
Bendig, J., Bolten, A., and Bareth, G.: UAV-based imaging for multi-temporal, very high resolution crop surface models to monitor crop growth variability, Photogramm. Fernerkun., 6, 551–562, doi:10.1127/1432-8364/2013/0200, 2013.
Bini, M., Isola, I., Pappalardo, M., Ribolini, A., Favalli, M., Ragaini, L., and Zanchetta, G.: Abrasive notches along the Atlantic Patagonian coast and their potential use as sea level markers: the case of Puerto Deseado (Santa Cruz, Argentina), Earth Surf. Proc. Land., 39, 1550–1558, doi:10.1002/esp.3612, 2014.
Bracken, L. J., Turnbull, L., Wainwright, J., and Bogaart, P.: State of science sediment connectivity: a framework for understanding sediment transfer at multiple scales, Earth Surf. Proc. Land., 40, 177–188, doi:10.1002/esp.3635, 2015.
Brasington, J., Vericat, D., and Rychkov, I.: Modeling river bed morphology, roughness, and surface sedimentology using high resolution terrestrial laser scanning, Water Resour. Res., 48, W11519, doi:10.1029/2012WR012223, 2012.
Bretar, F., Arab-Sedze, M., Champion, J., Pierrot-Deseilligny, M., Heggy, E., and Jacquemoud, S.: An advanced photogrammetric method to measure surface roughness: application to volcanic terrains in the Piton de la Fournaise, Reunion Island, Remote Sens. Environ., 135, 1–11, doi:10.1016/j.rse.2013.03.026, 2013.
Brothelande, E., Lénat, J.-F., Normier, A., Bacri, C., Peltier, A., Paris, R., Kelfoun, K., Merle, O., Finizola, A., and Garaebiti, E.: Insights into the evolution of the Yenkahe resurgent dome (Siwi caldera, Tanna Island, Vanuatu) inferred from aerial high-resolution photogrammetry, J. Volcanol. Geoth. Res., 299, 13 pp., doi:10.1016/j.jvolgeores.2015.04.006, 2015.
Brown, M. Z., Burschka, D., and Hager, G. D.: Advances in computational stereo, IEEE T. Pattern Anal., 25, 993–1008, 2003.
Buckley, S., Howell, J., Enge, H., and Kurz, T.: Terrestrial laser scanning in geology: data acquisition, processing and accuracy considerations, J. Geol. Soc. London, 165, 625–638, 2008.
Burns, J. H. R., Delparte, D., Gates, R. D., and Takabayashi, M.: Integrating structure-from-motion photogrammetry with geospatial software as a novel technique for quantifying 3D ecological characteristics of coral reefs, PeerJ, 3, e1077, doi:10.7717/peerj.1077, 2015.
Castillo, C., Pérez, R., James, M. R., Quinton, J. N., Taguas, E. V., and Gómez, J. A.: Comparing the accuracy of several field methods for measuring gully erosion, Soil Sci. Soc. Am. J., 76, 1319–1332, doi:10.2136/sssaj2011.0390, 2012.

ESURFD
3, 1445–1508, 2015

Castillo, C., Taguas, E. V., Zarco-Tejada, P., James, M. R., and Gómez, J. A.: The normalized topographic method: an automated procedure for gully mapping using GIS, Earth Surf. Proc. Land., 39, 2002–2015, doi:10.1002/esp.3595, 2014.
Castillo, C., James, M. R., Redel-Macías, M. D., Pérez, R., and Gómez, J. A.: SF3M software: 3-D photo-reconstruction for non-expert users and its application to a gully network, SOIL, 1, 583–594, doi:10.5194/soil-1-583-2015, 2015.
Cavalli, M., Tarolli, P., Marchi, L., and Fontana, G. D.: The effectiveness of airborne LiDAR data in the recognition of channel-bed morphology, Catena, 73, 249–260, doi:10.1016/j.catena.2007.11.001, 2008.
Chandler, J.: Effective application of automated digital photogrammetry for geomorphological research, Earth Surf. Proc. Land., 24, 51–63, 1999.
Cignoni, P., Callieri, M., Corsini, M., Dellepiane, M., Ganovelli, F., and Ranzuglia, G.: MeshLab: an open-source mesh processing tool, in: Eurographics Italian Chapter Conference, Salerno, Italy, 129–136, 2008.
Clapuyt, F., Vanacker, V., and Van Oost, K.: Reproducibility of UAV-based earth topography reconstructions based on Structure-from-Motion algorithms, Geomorphology, doi:10.1016/j.geomorph.2015.05.011, 2015.
Collier, P.: The impact on topographic mapping of developments in land and air survey: 1900–1939, Cartogr. Geogr. Inform., 29, 155–174, 2002.
Dandois, J. P. and Ellis, E. C.: High spatial resolution three-dimensional mapping of vegetation spectral dynamics using computer vision, Remote Sens. Environ., 136, 259–276, doi:10.1016/j.rse.2013.04.005, 2013.
Díaz-Varela, R., de la Rosa, R., León, L., and Zarco-Tejada, P.: High-resolution airborne UAV imagery to assess olive tree crown parameters using 3-D photo reconstruction: application in breeding trials, Remote Sensing, 7, 4213–4232, doi:10.3390/rs70404213, 2015.
Dietrich, J. T.: Riverscape mapping with helicopter-based structure-from-motion photogrammetry, Geomorphology, 252, 144–157, doi:10.1016/j.geomorph.2015.05.008, 2016.
Ducher, G.: Photogrammetry – the largest operational application of remote sensing, Photogrammetria, 41, 72–82, 1987.
East, A. E., Pess, G. R., Bountry, J. A., Magirl, C. S., Ritchie, A. C., Logan, J. B., Randle, T. J., Mastin, M. C., Minear, J. T., Duda, J. J., Liermann, M. C., McHenry, M. L., Beechie, T. J., and Shafroth, P. B.: Reprint of: large-scale dam removal on the Elwha River, Washing-

ESURFD
3, 1445–1508, 2015

ton, USA: river channel and floodplain geomorphic change, Geomorphology, 246, 687–708, doi:10.1016/j.geomorph.2015.04.027, 2015.
Eltner, A. and Baumgart, P.: Accuracy constraints of terrestrial Lidar data for soil erosion measurement: application to a mediterranean field plot, Geomorphology, 245, 243–254, doi:10.1016/j.geomorph.2015.06.008, 2015.
Eltner, A. and Schneider, D.: Analysis of different methods for 3-D reconstruction of natural surfaces from parallel-axes UAV images, Photogramm. Rec., 30, 279–299, doi:10.1111/phor.12115, 2015.
Eltner, A., Mulsow, C., and Maas, H.: Quantitative measurement of soil erosion from TLS and UAV data, Int. Arch. Photogramm. Rem. Sens., XL-1/W2, 119–124, 2013.
Eltner, A., Baumgart, P., Maas, H.-G., and Faust, D.: Multi-temporal UAV data for automatic measurement of rill and interrill erosion on loess soil, Earth Surf. Proc. Land., 40, 741–755, doi:10.1002/esp.3673, 2015.
Favalli, M., Fornaciai, A., Isola, I., Tarquini, S., and Nannipieri, L.: Multiview 3-D reconstruction in geosciences, Comput. Geosci., 44, 168–176, doi:10.1016/j.cageo.2011.09.012, 2012.
Fekete, S., Diederichs, M., and Lato, M.: Geotechnical and operational applications for 3-dimensional laser scanning in drill and blast tunnels, Tunn. Undergr. Sp. Tech., 25, 614–628, doi:10.1016/j.tust.2010.04.008, 2010.
Fernández, T., Pérez, J. L., Cardenal, F. J., López, A., Gómez, J. M., Colomo, C., Delgado, J., and Sánchez, M.: Use of a light UAV and photogrammetric techniques to study the evolution of a landslide in Jaén (Southern Spain), ISPRS, Int. Arch. Photogramm. Rem. Sens., XL-3/W3, 241–248, doi:10.5194/isprsarchives-XL-3-W3-241-2015, 2015.
Fischler, M. A. and Bolles, R. C.: Random sample consensus: a paradigm for model fitting with applications to image analysis and automated cartography, Commun. ACM, 24, 381–395, doi:10.1145/358669.358692, 1981.
Fonstad, M. A., Dietrich, J. T., Courville, B. C., Jensen, J. L., and Carbonneau, P. E.: Topographic structure from motion: a new development in photogrammetric measurement, Earth Surf. Proc. Land., 38, 421–430, doi:10.1002/esp.3366, 2013.
Frahm, J.-M., Pollefeys, M., Lazebnik, S., Gallup, D., Clipp, B., Raguram, R., Wu, C., Zach, C., and Johnson, T.: Fast robust large-scale mapping from video and internet photo collections, ISPRS J. Photogramm., 65, 538–549, doi:10.1016/j.isprsjprs.2010.08.009, 2010.

ESURFD
3, 1445–1508, 2015

Franceschi, M., Teza, G., Preto, N., Pesci, A., Galgaro, A., and Girardi, S.: Discrimination between marls and limestones using intensity data from terrestrial laser scanner, ISPRS J. Photogramm., 64, 522–528, doi:10.1016/j.isprsjprs.2009.03.003, 2009.

Francioni, M., Salvini, R., Stead, D., Giovannini, R., Riccucci, S., Vanneschi, C., and Gullì, D.: An integrated remote sensing-GIS approach for the analysis of an open pit in the Carrara marble district, Italy: slope stability assessment through kinematic and numerical methods, Comput. Geotech., 67, 46–63, doi:10.1016/j.compgeo.2015.02.009, 2015.

Frankl, A., Stal, C., Abraha, A., Nyssen, J., Rieke-Zapp, D., De Wulf, A., and Poesen, J.: Detailed recording of gully morphology in 3-D through image-based modelling PhotoScan Digital Elevation Model (DEM) soil pipes Structure from Motion–Multi View Stereo (SfM–MVS) volume calculation, Catena, 127, 92–101, doi:10.1016/j.catena.2014.12.016, 2014.

Furukawa, Y. and Ponce, J.: Accurate, dense, and robust multiview stereopsis, IEEE T. Pattern Anal., 83, 1362–1376, doi:10.1109/TPAMI.2009.161, 2010.

Furukawa, Y., Curless, B., Seitz, S. M., and Szeliski, R.: Towards internet-scale multi-view stereo, in: IEEE Conference on Computer Vision and Pattern Recognition, San Francisco, CA, USA, 13–18 June 2010, 1434–1441, doi:10.1109/CVPR.2010.5539802, 2010.

Genchi, S. A., Vitale, A. J., Perillo, G. M. E., and Delrieux, C. A.: Structure-from-motion approach for characterization of bioerosion patterns using UAV imagery, Sensors, 15, 3593–3609, doi:10.3390/s150203593, 2015.

Gienko, G. A. and Terry, J. P.: Three-dimensional modeling of coastal boulders using multi-view image measurements, Earth Surf. Proc. Land., 39, 853–864, doi:10.1002/esp.3485, 2014.

Gigli, G. and Casagli, N.: Semi-automatic extraction of rock mass structural data from high resolution LIDAR point clouds, Int. J. Rock Mech. Min., 48, 187–198, doi:10.1016/j.ijrmms.2010.11.009, 2011.

Girardeau-Montaut, D.: CloudCompare (version 2.x; GPL software), EDF RandD, Telecom ParisTech, available at: http://www.cloudcompare.org/, last access: 1 March 2015.

Gomez, C.: Digital photogrammetry and GIS-based analysis of the bio-geomorphological evolution of Sakurajima Volcano, diachronic analysis from 1947 to 2006, J. Volcanol. Geoth. Res., 280, 1–13, 2014.

Gomez, C., Hayakawa, Y., and Obanawa, H.: A study of Japanese landscapes using structure from motion derived DSMs and DEMs based on historical aerial photographs: new opportunities for vegetation monitoring and diachronic geomorphology, Geomorphology, 242, 11–20, doi:10.1016/j.geomorph.2015.02.021, 2015.

ESURFD
3, 1445–1508, 2015

Gómez-Gutiérrez, Á., de Sanjosé-Blasco, J. J., de Matías-Bejarano, J., and Berenguer-Sempere, F.: Comparing two photo-reconstruction methods to produce high density point clouds and DEMs in the Corral del Veleta rock glacier (Sierra Nevada, Spain), Remote Sensing, 6, 5407–5427, doi:10.3390/rs6065407, 2014a.

Gómez-Gutiérrez, Á., Schnabel, S., Berenguer-Sempere, F., Lavado-Contador, F., and Rubio-Delgado, J.: Using 3-D photo-reconstruction methods to estimate gully headcut erosion, Catena, 120, 91–101, doi:10.1016/j.catena.2014.04.004, 2014b.

Gómez-Gutiérrez, Á., de Sanjosé-Blasco, J., Lozano-Parra, J., Berenguer-Sempere, F., and de Matías-Bejarano, J.: Does HDR pre-processing improve the accuracy of 3-D models obtained by means of two conventional SfM-MVS software packages? The case of the Corral del Veleta rock glacier, Remote Sensing, 7, 10269–10294, doi:10.3390/rs70810269, 2015.

Gruen, A.: Development and status of image matching in photogrammetry, Photogramm. Rec., 27, 36–57, doi:10.1111/j.1477-9730.2011.00671.x, 2012.

Hartzell, P., Glennie, C., Biber, K., and Khan, S.: Application of multispectral LiDAR to automated virtual outcrop geology, ISPRS J. Photogramm., 88, 147–155, doi:10.1016/j.isprsjprs.2013.12.004, 2014.

Harwin, S. and Lucieer, A.: Assessing the accuracy of georeferenced point clouds produced via multi-view stereopsis from unmanned aerial vehicle (UAV) imagery, Remote Sensing, 4, 1573–1599, doi:10.3390/rs4061573, 2012.

Heritage, G. and Hetherington, D.: Towards a protocol for laser scanning in fluvial geomorphology, Earth Surf. Proc. Land., 32, 66–74, doi:10.1002/esp.1375, 2007.

Hirschmüller, H.: Semi-global matching – motivation, developments and applications, Photogrammetric Week, 11, 173–184, 2011.

Humair, F., Abellan, A., Carrea, D., Matasci, B., Epard, J.-L., and Jaboyedoff, M.: Geological layers detection and characterisation using high resolution 3-D point clouds: example of a box-fold in the Swiss Jura Mountains, Eur. J. Rem. Sens., 48, 541–568, doi:10.5721/EuJRS20154831, 2015.

Immerzeel, W. W., Kraaijenbrink, A., Shea, J. M., Shrestha, A. B., Pellicciotti, F., Bierkens, M. F. P., and De Jong, S. M.: High-resolution monitoring of Himalayan glacier dynamics using unmanned aerial vehicles, Remote Sens. Environ., 150, 93–103, doi:10.1016/j.rse.2014.04.025, 2014.

Jaboyedoff, M., Metzger, R., Oppikofer, T., Couture, R., Derron, M.-H., Locat, J., and Turmel, D.: New insight techniques to analyze rock-slope relief using DEM and 3-D-imaging cloud points:

ESURFD
3, 1445–1508, 2015

COLTOP-3D software, in: Rock Mechanics: Meeting Society's Challenges and Demands, 1st edn., edited by: Eberhardt, E., Stead, D., and Morrison, T., Taylor and Francis, London, 61–68, 2007.
Jackson, M. and Magro, G.: Real-time crowd-sourcing, data and modelling, in: IAIA15 Conference Proceedings, Florence, 20–23 April 2015, 6 pp., 2015.
James, M. R. and Robson, S.: Straightforward reconstruction of 3-D surfaces and topography with a camera: accuracy and geoscience application, J. Geophys. Res., 117, F03017, doi:10.1029/2011JF002289, 2012.
James, M. R. and Robson, S.: Mitigating systematic error in topographic models derived from UAV and ground-based image networks, Earth Surf. Proc. Land., 39, 1413–1420, doi:10.1002/esp.3609, 2014a.
James, M. R. and Robson, S.: Sequential digital elevation models of active lava flows from ground-based stereo time-lapse imagery, ISPRS J. Photogramm., 97, 160–170, doi:10.1016/j.isprsjprs.2014.08.011, 2014b.
James, M. R. and Varley, N.: Identification of structural controls in an active lava dome with high resolution DEMs: Volcán de Colima, Mexico, Geophys. Res. Lett., 39, L22303, doi:10.1029/2012GL054245, 2012.
Javernick, L., Brasington, J., and Caruso, B.: Modeling the topography of shallow braided rivers using Structure-from-Motion photogrammetry, Geomorphology, 213, 166–182, doi:10.1016/j.geomorph.2014.01.006, 2014.
Johnson, K., Nissen, E., Saripalli, S., Arrowsmith, J. R., Mcgarey, P., Scharer, K., Williams, P., and Blisniuk, K.: Rapid mapping of ultrafine fault zone topography with structure from motion, Geosphere, 10, 969, doi:10.1130/GES01017.1, 2014.
Johnson-Roberson, M., Bryson, M., Douillard, B., Pizarro, O., and Williams, S. B.: Discovering salient regions on 3-D photo-textured maps: crowdsourcing interaction data from multitouch smartphones and tablets, Comput. Vis. Image Und., 131, 28–41, doi:10.1016/j.cviu.2014.07.006, 2015.
Kääb, A.: Glacier volume changes using ASTER satellite stereo and ICESat GLAS laser altimetry. A test study on Edgeøya, Eastern Svalbard, IEEE T. Geosci. Remote, 46, 2823–2830, doi:10.1109/TGRS.2008.2000627, 2008.
Kääb, A., Girod, L., and Berthling, I.: Surface kinematics of periglacial sorted circles using structure-from-motion technology, The Cryosphere, 8, 1041–1056, doi:10.5194/tc-8-1041-2014, 2014.

ESURFD
3, 1445–1508, 2015

Kaiser, A., Neugirg, F., Rock, G., Müller, C., Haas, F., Ries, J., and Schmidt, J.: Small-scale surface reconstruction and volume calculation of soil erosion in complex Moroccan gully morphology using structure from motion, Remote Sensing, 6, 7050–7080, doi:10.3390/rs6087050, 2014.

Kaiser, A., Neugirg, F., Haas, F., Schmidt, J., Becht, M., and Schindewolf, M.: Determination of hydrological roughness by means of close range remote sensing, SOIL, 1, 613–620, doi:10.5194/soil-1-613-2015, 2015.

Khoshelham, K., Altundag, D., Ngan-Tillard, D., and Menenti, M.: Influence of range measurement noise on roughness characterization of rock surfaces using terrestrial laser scanning, Int. J. Rock Mech. Min., 48, 1215–1223, doi:10.1016/j.ijrmms.2011.09.007, 2011.

Kraus, K.: Photogrammetry: Geometry from Images and Laser Scans, 2nd edn., De Gruyter, Berlin, Germany, 459 pp., 2007.

Kromer, R., Abellán, A., Hutchinson, D., Lato, M., Edwards, T., and Jaboyedoff, M.: A 4-D filtering and calibration technique for small-scale point cloud change detection with a terrestrial laser scanner, Remote Sensing, 7, 13029–13052, doi:10.3390/rs71013029, 2015.

Lague, D., Brodu, N., and Leroux, J.: Accurate 3-D comparison of complex topography with terrestrial laser scanner: application to the Rangitikei canyon (N-Z), ISPRS J. Photogramm., 82, 10–26, doi:10.1016/j.isprsjprs.2013.04.009, 2013.

Laussedat, A.: La métrophotographie, Bibliothèque Photographique, Gauthier-Villars, Paris, 55 pages, 1899.

Lato, M., Hutchinson, J., Diederichs, M., Ball, D., and Harrap, R.: Engineering monitoring of rockfall hazards along transportation corridors: using mobile terrestrial LiDAR, Nat. Hazards Earth Syst. Sci., 9, 935–946, doi:10.5194/nhess-9-935-2009, 2009.

Leon, J. X., Roelfsema, C. M., Saunders, M. I., and Phinn, S. R.: Measuring coral reef terrain roughness using "Structure-from-Motion" close-range photogrammetry, Geomorphology, 242, 21–28, doi:10.1016/j.geomorph.2015.01.030, 2015.

Lim, M., Petley, D. N., Rosser, N. J., Allison, R. J., Long, A. J., and Pybus, D.: Combined digital photogrammetry and time-of-flight laser scanning for monitoring cliff evolution, Photogramm. Rec., 20, 109–129, 2008.

Lowe, D. G.: Object recognition from local scale-invariant features, in: The Proceedings of the 7th IEEE International Conference on Computer Vision, 20–27 September 1999, 2, 1150–1157, 1999.

ESURFD
3, 1445–1508, 2015

Lowe, D. G.: Distinctive image features from scale-invariant keypoints, Int. J. Comput. Vision, 60, 91–110, doi:10.1023/B:VISI.0000029664.99615.94, 2004.
Lucieer, A., de Jong, S., and Turner, D.: Mapping landslide displacements using Structure from Motion (SfM) and image correlation of multi-temporal UAV photography, Prog. Phys. Geog., 38, 1–20, doi:10.1177/0309133313515293, 2013.
Lucieer, A., Turner, D., King, D. H., and Robinson, S. A.: Using an unmanned aerial vehicle (UAV) to capture micro-topography of antarctic moss beds, Int. J. Appl. Earth Obs., 27, 53–62, doi:10.1016/j.jag.2013.05.011, 2014.
Luhmann, T., Robson, S., Kyle, S., and Boehm, J.: Close-Range Photogrammetry and 3-D Imaging, 2nd edn., De Gruyter, Berlin, Germany, 683 pp., 2014.
Mancini, F., Dubbini, M., Gattelli, M., Stecchi, F., Fabbri, S., and Gabbianelli, G.: Using unmanned aerial vehicles (UAV) for high-resolution reconstruction of topography: the structure from motion approach on coastal environments, Remote Sensing, 5, 6880–6898, doi:10.3390/rs5126880, 2013.
Martin-Brualla, R., Gallup, D., and Seitz, S. M.: Time-lapse mining from internet photos, ACM Transactions on Graphics (TOG), 34, 62, 2015.
Meesuk, V., Vojinovic, Z., Mynett, A. E., and Abdullah, A. F.: Urban flood modelling combining top-view LiDAR data with ground-view SfM observations, Adv. Water Resour., 75, 105–117, doi:10.1016/j.advwatres.2014.11.008, 2015.
Micheletti, N., Chandler, J. H., and Lane, S. N.: Investigating the geomorphological potential of freely available and accessible structure-from-motion photogrammetry using a smartphone, Earth Surf. Proc. Land., 40, 473–486, doi:10.1002/esp.3648, 2014.
Micheletti, N., Chandler, J. H., and Lane, S. N.: Structure from Motion (SfM) Photogrammetry, in: Geomorphological Techniques (Online Edition), edited by: Cook, S. J., Clarke, L. E., and Nield, J. M., British Society for Geomorphology, London, ISSN: 2047-0371, 2015.
Michoud, C., Carrea, D., Costa, S., Derron, M.-H., Jaboyedoff, M., Delacourt, C., Maquaire, O., Letortu, P., and Davidson, R.: Landslide detection and monitoring capability of boat-based mobile laser scanning along Dieppe coastal cliffs, Normandy, Landslides, 12, 403–418, 2015.
Mikhail, E., Bethel, J., and McGlone, J.: Introduction to Modern Photogrammetry, John Wiley and Sons, Inc., New York, 479 pp., 2001.

ESURFD
3, 1445–1508, 2015

Mikolajczyk, K., Tuytelaars, T., Schmid, C., Zisserman, A., Matas, J., Schaffalitzky, F., Kadir, T., and Van Gool, L.: A comparison of affine region detectors, Int. J. Comput. Vision, 65, 43–72, doi:10.1007/s11263-005-3848-x, 2005.

Milan, D. J., Heritage, G. L., and Hetherington, D.: Assessment of erosion and deposition volumes and channel change application of a 3-D laser scanner in the assessment of erosion and deposition volumes and channel change in a proglacial river, Earth Surf. Proc. Land., 32, 1657–1674, doi:10.1002/esp.1592, 2007.

Monserrat, O. and Crosetto, M.: Deformation measurement using terrestrial laser scanning data and least squares 3-D surface matching, ISPRS J. Photogramm., 63, 142–154, doi:10.1016/j.isprsjprs.2007.07.008, 2008.

Morgenroth, J. and Gomez, C.: Assessment of tree structure using a 3-D image analysis technique – a proof of concept, Urban For. Urban Gree., 13, 198–203, doi:10.1016/j.ufug.2013.10.005, 2014.

Nadal-Romero, E., Revuelto, J., Errea, P., and López-Moreno, J. I.: The application of terrestrial laser scanner and SfM photogrammetry in measuring erosion and deposition processes in two opposite slopes in a humid badlands area (central Spanish Pyrenees), SOIL, 1, 561–573, doi:10.5194/soil-1-561-2015, 2015.

Nolan, M., Larsen, C. F., and Sturm, M.: Mapping snow-depth from manned-aircraft on landscape scales at centimeter resolution using Structure-from-Motion photogrammetry, The Cryosphere Discuss., 9, 333–381, doi:10.5194/tcd-9-333-2015, 2015.

Nouwakpo, S. K., James, M. R., Weltz, M. A., Huang, C.-H., Chagas, I., and Lima, L.: Evaluation of structure from motion for soil microtopography measurement, Photogramm. Rec., 29, 297–316, doi:10.1111/phor.12072, 2014.

Nouwakpo, S. K., Weltz, M. A., and McGwire, K.: Assessing the performance of structure-from-motion photogrammetry and terrestrial lidar for reconstructing soil surface microtopography of naturally vegetated plots, Earth Surf. Proc. Land., doi:10.1002/esp.3787, 2015.

Oppikofer, T., Jaboyedoff, M., Blikra, L., Derron, M.-H., and Metzger, R.: Characterization and monitoring of the Åknes rockslide using terrestrial laser scanning, Nat. Hazards Earth Syst. Sci., 9, 1003–1019, doi:10.5194/nhess-9-1003-2009, 2009.

Ouédraogo, M. M., Degré, A., Debouche, C., and Lisein, J.: The evaluation of unmanned aerial system-based photogrammetry and terrestrial laser scanning to generate DEMs of agricultural watersheds, Geomorphology, 214, 339–355, doi:10.1016/j.geomorph.2014.02.016, 2014.

Passalacqua, P., Belmont, P., Staley, D. M., Simley, J. D., Arrowsmith, J. R., Bode, C. A., Crosby, C., DeLong, S. B., Glenn, N. F., Kelly, S. A., Lague, D., Sangireddy, H., Schaffrath, K., Tarboton, D. G., Wasklewicz, T., and Wheaton, J. M.: Analyzing high resolution topography for advancing the understanding of mass and energy transfer through landscapes: a review, Earth-Sci. Rev., 148, 174–193, doi:10.1016/j.earscirev.2015.05.012, 2015.

Pears, N., Liu, Y., and Bunting, P.: 3-D Imaging, Analysis and Applications, Springer, London, 499 pp., 2012.

Piermattei, L., Carturan, L., and Guarnieri, A.: Use of terrestrial photogrammetry based on structure from motion for mass balance estimation of a small glacier in the Italian Alps, Earth Surf. Proc. Land., 40, 1791–1802, doi:10.1002/esp.3756, 2015.

Pierrot-Deseilligny, M. and Clery, I.: APERO, an open source bundle adjustment software for automatic calibration and orientation of set of images, Intern. Arch. Photogramm. Rem. Sens., 38–5, 269–276, 2011.

Pierrot-Deseilligny, M. and Clery, I.: Some Possible Protocols of Acquisition for the Optimal Use of the "Apero" Open Source Software in Automatic Orientation and Calibration, EuroCow 2012, Barcelona, Spain, 10 pp., 2012.

Pollyea, R. and Fairley, J.: Estimating surface roughness of terrestrial laser scan data using orthogonal distance regression, Geology, 39, 623–626, doi:10.1130/G32078.1, 2011.

Poropat, G.: Measurement of surface roughness of rock discontinuities, in: Proc. of the 3rd CANUS Rock Mechanics Symposium, Toronto, 3976, 2009.

Prosdocimi, M., Calligaro, S., Sofia, G., Dalla Fontana, G., and Tarolli, P.: Bank erosion in agricultural drainage networks: new challenges from Structure-from-Motion photogrammetry for post-event analysis, Earth Surf. Proc. Land., 40, 1891–1906, doi:10.1002/esp.3767, 2015.

Remondino, F., Spera, M. G., Nocerino, E., Menna, F., and Nex, F.: State of the art in high density image matching, Photogramm. Rec., 29, 144–166, doi:10.1111/phor.12063, 2014.

Rippin, D. M., Pomfret, A., and King, N.: High resolution mapping of supraglacial drainage pathways reveals link between micro-channel drainage density, surface roughness and surface reflectance, Earth Surf. Proc. Land., 40, 1279–1290, doi:10.1002/esp.3719, 2015.

Royan, M., Abellan, A., and Vilaplana, J.: Progressive failure leading to the 3 December 2013 rockfall at Puigcercós scarp (Catalonia, Spain), Landslides, 12, 585–595, 2015.

Sanz-Ablanedo, E., Rodríguez-Pérez, J. R., Armesto, J., and Taboada, M. F. Á.: Geometric stability and lens decentering in compact digital cameras, Sensors, 10, 1553–1572 doi:10.3390/s100301553, 2010.

ESURFD
3, 1445–1508, 2015

Schaffalitzky, F. and Zisserman, A.: Multi-view matching for unordered image sets, or "How do I organize my holiday snaps?", Lect. Notes Comput. Sci., 2350, 414–431, doi:10.1007/3-540-47969-4, 2002.

Shortis, M. R., Bellman, C. J., Robson, S., Johnston, G. J., and Johnson, G. W.: Stability of zoom and fixed lenses used with digital SLR cameras, Intern. Arch. Photogramm. Rem. Sens., XXXVI, 285–290, 2006.

Siebert, S. and Teizer, J.: Mobile 3-D mapping for surveying earthwork projects using an unmanned aerial vehicle (UAV) system, Automat. Constr., 41, 1–14, doi:10.1016/j.autcon.2014.01.004, 2014.

Smith, M. W. and Vericat, D.: From experimental plots to experimental landscapes: topography, erosion and deposition in sub-humid badlands from structure-from-motion photogrammetry, Earth Surf. Proc. Land., 40, 1656–1671, doi:10.1002/esp.3747, 2015.

Smith, M. W., Carrivick, J. L., Hooke, J., and Kirkby, M. J.: Reconstructing flash flood magnitudes using "structure-from-motion": a rapid assessment tool, J. Hydrol., 519, 1914–1927, doi:10.1016/j.jhydrol.2014.09.078, 2014.

Snapir, B., Hobbs, S., and Waine, T. W.: Roughness measurements over an agricultural soil surface with Structure from Motion, ISPRS J. Photogramm., 96, 210–223, doi:10.1016/j.isprsjprs.2014.07.010, 2014.

Snavely, N., Seitz, S. M., and Szeliski, R.: Photo tourism?: exploring photo collections in 3-D, ACM T. Graphic., 25, 835–846, 2006.

Snavely, N., Seitz, S. M., and Szeliski, R.: Modeling the world from internet photo collections, Int. J. Comput. Vision, 80, 189–210, doi:10.1007/s11263-007-0107-3, 2008.

Stöcker, C., Eltner, A., and Karrasch, P.: Measuring gullies by synergetic application of UAV and close range photogrammetry – a case study from Andalusia, Spain, Catena, 132, 1–11, doi:10.1016/j.catena.2015.04.004, 2015.

Stumpf, A., Malet, J.-P., Allemand, P., Pierrot-Deseilligny, M., and Skupinski, G.: Ground-based multi-view photogrammetry for the monitoring of landslide deformation and erosion, Geomorphology, 231, 130–145, doi:10.1016/j.geomorph.2014.10.039, 2014.

Sturzenegger, M. and Stead, D.: Close-range terrestrial digital photogrammetry and terrestrial laser scanning for discontinuity characterization on rock cuts, Eng. Geol., 106, 163–182, doi:10.1016/j.enggeo.2009.03.004, 2009.

ESURFD

3, 1445–1508, 2015

Tamminga, A. D., Eaton, B. C., and Hugenholtz, C. H.: UAS-based remote sensing of Wuvial change following an extreme Wood event, Earth Surf. Proc. Land., 40, 1464–1476, doi:10.1002/esp.3728, 2015.
Thomsen, L. M., Baartman, J. E. M., Barneveld, R. J., Starkloff, T., and Stolte, J.: Soil surface roughness: comparing old and new measuring methods and application in a soil erosion model, SOIL, 1, 399–410, doi:10.5194/soil-1-399-2015, 2015.
Tonkin, T. N., Midgley, N. G., Graham, D. J., and Labadz, J. C.: The potential of small unmanned aircraft systems and structure-from-motion for topographic surveys: a test of emerging integrated approaches at Cwm Idwal, North Wales, Geomorphology, 226, 35–43, doi:10.1016/j.geomorph.2014.07.021, 2014.
Torres-Sánchez, J., López-Granados, F., Serrano, N., Arquero, O., and Peña, J. M.: High-throughput 3-D monitoring of agricultural-tree plantations with unmanned aerial vehicle (UAV) technology, PLOS One, 10, e0130479, doi:10.1371/journal.pone.0130479, 2015.
Turner, D., Lucieer, A., and de Jong, S.: Time series analysis of landslide dynamics using an unmanned aerial vehicle (UAV), Remote Sensing, 7, 1736–1757, doi:10.3390/rs70201736, 2015.
Ullman, S.: The interpretation of structure from motion, P. R. Soc. B, 203, 405–426, 1979.
Vasuki, Y., Holden, E. J., Kovesi, P., and Micklethwaite, S.: Semi-automatic mapping of geological Structures using UAV-based photogrammetric data: an image analysis approach, Comput. Geosci., 69, 22–32, doi:10.1016/j.cageo.2014.04.012, 2014.
Westoby, M. J., Brasington, J., Glasser, N. F., Hambrey, M. J., and Reynolds, J. M.: "Structure-from-motion" photogrammetry: a low-cost, effective tool for geoscience applications, Geomorphology, 179, 300–314, doi:10.1016/j.geomorph.2012.08.021, 2012.
Westoby, M. J., Glasser, N. F., Hambrey, M. J., Brasington, J., Reynolds, J. M., and Hassan, M. A. A. M.: Reconstructing historic glacial lakeoutburst floods through numerical modelling and geomorphological assessment: extreme events in the Himalaya, Earth Surf. Proc. Land., 39, 1675–1692, doi:10.1002/esp.3617, 2014.
Woodget, A. S., Carbonneau, P. E., Visser, F., and Maddock, I. P.: Quantifying submerged fluvial topography using hyperspatial resolution UAS imagery and structure from motion photogrammetry, Earth Surf. Proc. Land., 40, 47–64, doi:10.1002/esp.3613, 2015.
Wu, C.: Towards linear-time incremental structure from motion, in: International Conference on 3-D Vision – 3-DV, Seattle, WA, USA, 29 June –1 July 2013, 127–134, 2013.

ESURFD
3, 1445–1508, 2015

Wu, C.: Critical configurations for radial distortion self-calibration, IEEE Conference on Computer Vision and Pattern Recognition (CVPR), 23–28 June 2014, 25–32, doi:10.1109/CVPR.2014.11, 2014.

Zarco-Tejada, P. J., Diaz-Varela, R., Angileri, V., and Loudjani, P.: Tree height quantification using very high resolution imagery acquired from an unmanned aerial vehicle (UAV) and automatic 3-D photo-reconstruction methods, Eur. J. Agron., 55, 89–99, doi:10.1016/j.eja.2014.01.004, 2014.

ESURFD

3, 1445–1508, 2015

Table 1. Nomenclature and brief definitions of image-based 3-D reconstruction related terms.

Image-based 3-D reconstruction	recording of the three-dimensional shape of an object from overlapping images from different perspectives
Computer Vision	algorithmic efforts to imitate human vision with focus on automation, amongst others, to reconstruct 3-D scenes with methods of image processing and image understanding
Structure from Motion (SfM)	fully automatic reconstruction of 3-D scenes from 2-D images in an arbitrary coordinate system
Photogrammetry	algorithmic efforts to determine 3-D model coordinates focussing on their accuracy and the precise measurement in images
SfM photogrammetry	fully automatic reconstruction of 3-D scenes from 2-D images with option to set parameters for (photogrammetric) optimisation of accuracy and precision
Dense matching	increase of resolution of point clouds that model 3-D scenes by pixel- or patch-wise matching in images of known intrinsic and extrinsic parameters
Stereo matching	reconstruction of object point through matching (in image space, Remondino et al., 2014) between two overlapping images
Multi-View-Stereo (MVS) matching	reconstruction of object point through matching (in object space, Remondino et al., 2014) from multiple overlapping images
Extrinsic parameters	exterior camera geometry comprising position (three shifts) and orientation (three rotations) of the camera projection centre
Intrinsic parameters	interior camera geometry comprising principle distance (distance between projection centre and image sensor), principle point (intersection of perpendicular from projection centre onto image plane) and distortion parameters (e.g. radial distortion)
Bundle block adjustment (BBA)	least-square optimisation to simultaneously solve for extrinsic (and intrinsic) parameters of all images; the term bundle correlates to rays that derive from 3-D points, converge in corresponding projection centres and intersect with image sensor
Camera self-calibration	intrinsic camera parameters are included as additional unknowns into BBA to solve for interior camera geometry
Ground Control Point (GCP)	in images clearly distinguishable point whose object coordinates are known to geo-reference surface model
Digital Elevation Model (DEM)	3-D description of the surface in either raster (grid) or vector (mesh) format
Point cloud	quantity of points of 3-D coordinates describing the surface within arbitrary or geo-referenced coordinate system, additional information such as normals or colours possible

ESURFD
3, 1445–1508, 2015

Table 2. Overview of the publication history divided in the main topics from 2012 until editorial deadline in September 2015. Several publications examined more than one topic resulting in a larger number of topics (number without brackets) than actual publications (number in brackets).

Year Topic	2012	2013	2014	2015	
Soil science	1	–	5	8	14
Volcanology	4	1	1	1	7
Glaciology	–	–	4	3	7
Mass movements	–	1	–	3	4
Fluvial morphology	–	1	6	4	11
Coastal morphology	3	1	3	–	7
Others	3	2	8	5	18
Topics (publications)	10 (7)	6 (6)	27 (24)	24 (24)	68 (61)

ESURFD
3, 1445–1508, 2015

Table 3. Different perspectives/platforms used for image acquisition of all 62 reviewed studies.

	Terrestrial	UAV	Manned aircraft
Number of applications	34	27	5

ESURFD
3, 1445–1508, 2015

Table 4. Parameters of a standard protocol for error assessment independent from individual study design.

	parameters
object	scale of study area, distance to object, ground sampling distance
camera	camera, sensor resolution, sensor size, pixel size, focal length
image acquisition	illumination condition, image number, overlap and/or baseline, image configuration and/or perspective
ground control	GCP type, GCP measurement (digital and reality), GCP number, GCP accuracy
data processing	Software, referencing implementation (one- or two-staged), output type
error assessment	reference type, reference error, error measure (e.g. M3C2, raster, ...), statistical value (e.g. RMSE, ...), registration residual
transferable ratios	relative error ratio (error/measuring distance), superior accuracy ratio (reference error/reconstruction error)

ESURFD
3, 1445–1508, 2015

Table A1. Summarises information about reviewed studies used for application evaluation and performance assessment of SfM photogrammetry.

Author	Year	Application	Software	Perspective	Distance [m]	Scale* [m]	Pixel size [µm]	Image number	Tool complex.	Measur. Error [mm]	Error ratio	Superior reference ratio	Theoret. error ratio
Bemis et al.	2014	structural geology	PhotoScan	UAV, terrestrial	–	–	–	–	–	–	–	–	–
Bendig et al.	2013	crop growth	PhotoScan	UAV	30	7	–	–	–	–	–	–	–
Bini et al.	2014	coast erosion/abrasion	Bundler	terrestrial	–	–	–	–	–	–	–	–	–
Bretar et al.	2013	(volcanic) surface roughness	APERO + MicMac	terrestrial	1.5	5.9–24.6	–	–	–	–	–	–	–
Brothelande et al.	2015	post-caldera resurgence	PhotoScan	aircraft	150	6000	*8.2*	7000	–	3100	48	62	–
Burns et al.	2015	coral reef	Photoscan	terrestrial (marine)	2	28	–	–	–	–	–	–	–
Castillo et al.	**2012**	**gully erosion**	**Bundler + PMVS2**	**terrestrial**	**7**	**7**	**5.2**	**191**	**basic**	**20**	**350**	**–**	**79**
Castillo et al.	**2014**	**ephemeral gully erosion**	**Bundler + PMVS2**	**terrestrial**	**6**	**25**	**5.2**	**515**	**basic**	**22**	**273**	**11**	**101**
Castillo et al.	**2015**	**gully erosion**	**SF3M**	**terrestrial**	**10**	**350**	**1.5**	**3095**	**basic**	**69**	**145**	**3.45**	**455**
Clapuyt et al.	2015	slope morphology	VisualSFM	UAV	50	100	–	–	–	–	–	–	–
Dandois and Ellis	2013	vegetation mapping	Photoscan	UAV	130	250	–	–	–	–	–	–	–
Dietrich	**2016**	**riverscape mapping**	**PhotoScan**	**helicopter**	**200**	**10 000**	***4.3***	**1483**	**complex**	**730**	**274**	**–**	**–**
Eltner et al.	**2015**	**soil erosion**	**Pix4D**	**UAV**	**10**	**30**	**2.0, 5.0**	**100**	**complex**	**5, 6**	**2000, 1667**	**–**	**–**
Eltner and Schneider	**2015**	**soil roughness**	**VisualSfM + PMVS2, PhotoScan, Pix4D, APERO + MicMac, Bundler + PMVS2**	**UAV**	**12**	**15**	**5.0**	**13**	**basic, complex**	**8.1–9.8**	**1224–1481**	**–**	**–**
Favalli et al.	**2012**	**geological outcrops, volcanic bomb, stalagmite**	**Bundler + PMVS2**	**terrestrial**	**1**	**0.1–0.3**	***5.2***	**30–67**	**basic**	**0.3–3.8**	**367–3333**	**–**	**–**
Fernández et al.	2015	landslide	Photoscan	UAV	90	250	–	–	–	–	–	–	–
Fonstad et al.	**2013**	**bedrock channel and floodplain**	**Photosynth (Bundler implementation)**	**terrestrial**	**40**	**200**	***1.7***	**304**	**basic**	**250**	**160**	**2**	**139**
Frankl et al.	**2015**	**gully measurement**	**PhotoScan**	**terrestrial**	**2**	**10**	***5.2***	**180–235**	**complex**	**17–190**	**11–147**	**0–4**	**156–2184**
Genchi et al.	**2015**	**bioerosion pattern**	**VisualSfM + PMVS2**	**UAV**	**20**	**100**	***1.5***	**400**	**basic**	**35**	**571**	**–**	**29**
Gienko and Terry	2014	coastal boulders	Photoscan	terrestrial	3	2.5	–	–	–	–	–	–	–
Gomez	2014	volcano morphology	Photoscan	aircraft	–	10 000	–	–	–	–	–	–	–
Gómez-Gutiérrez et al.	**2014**	**gully headcut**	**123D catch**	**terrestrial**	**9.3–10.5**	**10**	***4.3***	**41–93**	**basic**	**12–32**	**291–792**	**–**	**31–85**
Gómez-Gutiérrez et al.	**2014**	**rock glacier**	**123D catch**	**terrestrial**	**300**	**130**	***8.2***	**6**	**basic**	**430**	**698**	**72**	**103**
Gómez-Gutiérrez et al.	**2015**	**rock glacier**	**123D catch, PhotoScan**	**terrestrial**	**300**	**130**	***8.2***	**9**	**basic, complex**	**84–1029**	**–**	**–**	**–**
Harwin and Lucieer	2012	coastal erosion	Bundler + PMVS2	UAV	120	100	–	1	–	–	–	–	–
Immerzeel et al.	**2014**	**dynamic of debris coverd glacial tongue**	**PhotoScan**	**UAV**	**300**	**3500**	***1.3***	**284, 307**	**complex**	**330**	**909**	**–**	**–**
James and Robson	**2012**	**volcanic bomb, summit crater, coastal cliff**	**Bundler + PMVS2**	**terrestrial, UAV**	**0.7–1000**	**0.1–1600**	***5.2, 7.4***	**133–210**	**basic**	**1000–2333**	**0–62**	**1–12**	**16–25**
James and Varley	2012	volcanic dome control	Bundler Photogrammetry package	aircraft	505–2420	250	–	–	–	–	–	–	–
Javernick et al.	**2014**	**braided river**	**PhotoScan**	**helicopter**	**700**	**1500**	**–**	**147**	**complex**	**170**	**4118**	**3**	**–**
Johnson et al.	**2014**	**alluvial fan, earthquake scarp**	**PhotoScan**	**UAV**	**50, 60**	**300, 1000**	***4.8***	**233. 450**	**complex**	**130–410**	**122–385**	**–**	**–**
Kaiser et al.	**2014**	**gully and rill erosion**	**PhotoScan**	**terrestrial**	**5**	**10**	**6.4**	**–**	**complex**	**73–141**	**35–68**	**–**	**232–447**

ESURFD
3, 1445–1508, 2015

Table A1. Continued.

Author	Year	Application	Software	Perspective	Distance [m]	Scale* [m]	Pixel size [µm]	Image number	Tool complex.	Measur. Error [mm]	Error ratio	Superior reference ratio	Theoret. error ratio
Kaiser et al.	2015	soil hydraulic roughness	PhotoScan	terrestrial	0.5	1	–	–	–	–	–	–	–
Leon et al.	**2015**	**coral reef roughness**	**PhotoScan**	**terrestrial (marine)**	**1.5**	**250**	***1.5***	**1370**	**complex**	**0.6**	**2500**	**–**	**–**
Lucieer et al.	2013	landslide	PhotoScan	UAV	40	125	–	–	–	–	–	–	–
Lucieer et al.	2014	antartic moss beds	PhotoScan	UAV	50	64	–	–	–	–	–	–	–
Mancini et al.	**2013**	**fore dune**	**PhotoScan**	**UAV**	**40**	**200**	***4.3***	**550**	**complex**	**110–190**	**211–364**	**4**	**–**
Meesuk et al.	2014	Urban flooding	VisualSfM	terrestrial	–	–	–	–	–	–	–	–	–
Micheletti et al.	**2014**	**river bank, alluvial fan**	**123D Catch**	**terrestrial**	**10, 345**	**10, 300**	***4.8, 1.8***	**13**	**complex**	**16.8–526.3**	**327–595**	**–**	**40–73**
Morgenroth and Gomez	2014	tree structure	Photoscan	terrestrial	5	5	–	–	–	–	–	–	–
Nadal-Romero et al.	**2015**	**badland erosion**	**PhotoScan**	**terrestrial**	**50, 125**	**50, 100**	***5.5***	**15, 17**	**complex**	**14–33**	**2500–4032**	**1–2**	**6–10**
Nouwakpo et al.	2014	soil microtopography	PhotoScan	terrestrial	3.1	10	–	–	–	–	–	–	–
Nouwakpo et al.	**2015**	**microtopography erosion plots**	**PhotoScan**	**terrestrial**	**2**	**6**	***6.4***	**25**	**complex**	**5**	**400**	**–**	**–**
Ouédraogo et al.	**2014**	**agricultural watershed**	**Apero + MicMac, PhotoScan**	**UAV**	**100**	**200**	***2.0***	**760**	**complex**	**90, 139**	**1111, 719**	**–**	**6, 9**
Piermattei et al.	**2015**	**debris covered glacier monitoring**	**PhotoScan**	**terrestrial**	**100**	**350**	***4.8, 6.3***	**35, 47**	**complex**	**300, 130**	**333, 769**	**2, 1**	**56, 35**
Prosdocimi et al.	**2015**	**channel bank erosion**	**PhotoScan**	**terrestrial**	**7**	**30**	***1.4–6.3***	**60**	**complex**	**57–78**	**90–123**	**1**	**143–373**
Rippin et al.	**2015**	**supra-glacial hydrology**	**PhotoScan**	**UAV**	**121**	**2000**	***2.2***	**423**	**complex**	**400**	**303**	**–**	**–**
Ruzic et al.	**2014**	**coastal cliff**	**Autodesk ReCap**	**terrestrial**	**15**	**50**	***2.0***	**250**	**basic**	**70**	**214**	**1**	**82**
Smith et al.	**2014**	**post-flash flood evaluation**	**PhotoScan**	**terrestrial**	**50**	**150**	***1.7***	**–**	**complex**	**135**	**370**	**14**	**39**
Smith and Vericat	**2015**	**badland changes at different scales**	**PhotoScan**	**terrestrial, UAV, AutoGiro**	**5–250**	**20–1000**	***1.7, 5.5***	**30–527**	**complex**	**12.8–445**	**132–974**	**2–89**	**36–107**
Snapir et al.	**2014**	**roughness of soil surface**	**SfMToolkit**	**terrestrial**	**0.6**	**3**	***4.3***	**700**	**basic**	**2.7**	**222**	**270**	**–**
Stöcker et al.	2015	gully erosion	APERO + MicMac	terrestrial + UAV	2 + 15	35	–	–	–	–	–	–	–
Stumpf et al.	**2014**	**landslide scarp**	**VisualSfM + CMVS, APERO + MicMac**	**terrestrial**	**50**	**750**	***8.5***	**88–401**	**basic, complex**	**27–232**	**667–1852**	**1–3**	**13–64**
Tamminga et al.	**2015**	**change detection after extreme flood event**	**EnsoMOSAIC UAV**	**UAV**	**100**	**200**	***1.3***	**310**	**complex**	**47**	**2128**	**2**	**–**
Tonkin et al.	**2014**	**moraine-mound topography**	**PhotoScan**	**UAV**	**100**	**500**	***4.3***	**543**	**complex**	**517**	**193**	**–**	**–**
Torres-Sánchez et al.	2015	tree plantation	Photoscan	UAV	50, 100	–	–	–	–	–	–	–	–
Turner et al.	2012	antartic moss beds	Bundler + PMVS2	UAV	50	–	–	–	–	–	–	–	–
Turner et al.	**2015**	**landslide change detection**	**PhotoScan**	**UAV**	**40**	**125**	***4.3***	**62–415**	**complex**	**31–90**	**444–1290**	**1–3**	**–**
Vasuki et al.	2014	structural geology	Bundler + PMVS2	UAV	30–40	100	–	–	–	–	–	–	–
Westoby et al.	**2012**	**coastal cliff**	**SfMToolkit**	**terrestrial**	**15**	**300**	***4.3***	**889**	**basic**	**500**	**100**	**–**	**–**
Westoby et al.	**2014**	**moraine dam, alluvial debris fan**	**SfMToolkit3**	**terrestrial**	**500**	**500**	***4.3***	**1002, 1054**	**basic**	**814, 85**	**614, 1176**	**2, 43**	**–**
Woodget et al.	**2015**	**fluvial topography**	**PhotoScan**	**UAV**	**26–28**	**50, 100**	***2.0***	**32–64**	**complex**	**19–203**	**138–1421**	**–**	**–**
Zarco-Tejada et al.	**2014**	**tree height estimation**	**Pix4D**	**UAV**	**200**	**1000**	***4.3***	**1409**	**complex**	**350**	**571**	**23**	**–**

These studies are considered for performance analysis.
For most authors not all camera parameters are given. Hence, camera parameters are retrieved from dpreview.com (or similar sources).
* If scale or distance is not given, they are estimated from study area display.

ESURFD
3, 1445–1508, 2015

Table B1. Summarises non-commercial software tools beneficial for SfM photogrammetry processing and post-processing.

Name	Type	Website	Operative system	Functionalites
Bundler	Open Source	http://www.cs.cornell.edu/$~$snavely/bundler/	Linux Windows	Sparse 3-D reconstruction
VisualSFM	Freely-available	http://ccwu.me/vsfm/	Linux Mac Windows	Sparse and dense 3-D reconstruction Geo-referencing point clouds
PMVS2/CMVS	Open Source	http://www.di.ens.fr/pmvs/ http://www.di.ens.fr/cmvs/	Linux Windows	Dense 3-D reconstruction
SfMToolkit	Open Source	http://www.visual-experiments.com/demos/sfmtoolkit/	Windows	Sparse and dense 3-D reconstruction
APERO + MicMac	Open Source	http://logiciels.ign.fr/?Micmac	Linux Mac Windows	Sparse and dense 3-D reconstruction Geo-referencing Post-processing
Sfm_georef	Freely-available	http://www.lancaster.ac.uk/staff/jamesm/software/sfm_georef.htm	Windows	Geo-referencing point clouds
CloudCompare	Open Source	http://www.danielgm.net/cc/	Linux Mac Windows	Cloud processing
Meshlab	Open Source	http://meshlab.sourceforge.net/	Mac Windows	Cloud processing
Sf3M	Freely-available	http://sf3mapp.csic.es/	Windows	Sparse and dense 3-D reconstruction (Visual SfM) Geo-referencing (sfm-georef) Basic post-processing (CloudCompare)

ESURFD
3, 1445–1508, 2015

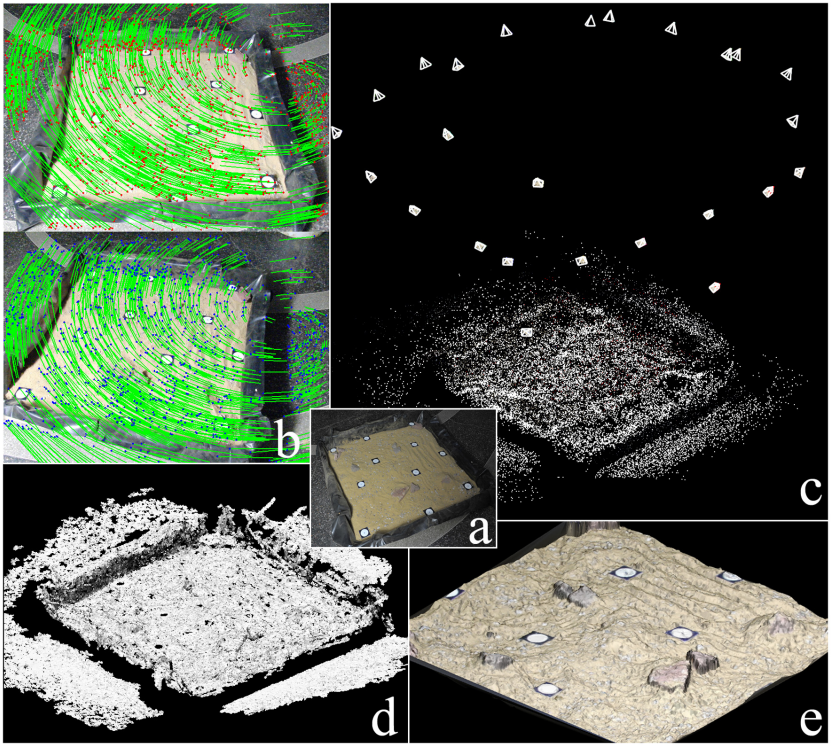

Figure 1. Exemplary workflow of image-based 3-D reconstruction: **(a)** illustration of a micro-plot (1 m^2), **(b)** matched-image pair with homologous points, **(c)** reconstructed image network geometry with sparse point cloud, **(d)** dense-matched point cloud, **(e)** meshed DEM of micro-plot.

ESURFD
3, 1445–1508, 2015

Figure 2. Map of the research sites of all studies of this review.

ESURFD
3, 1445–1508, 2015

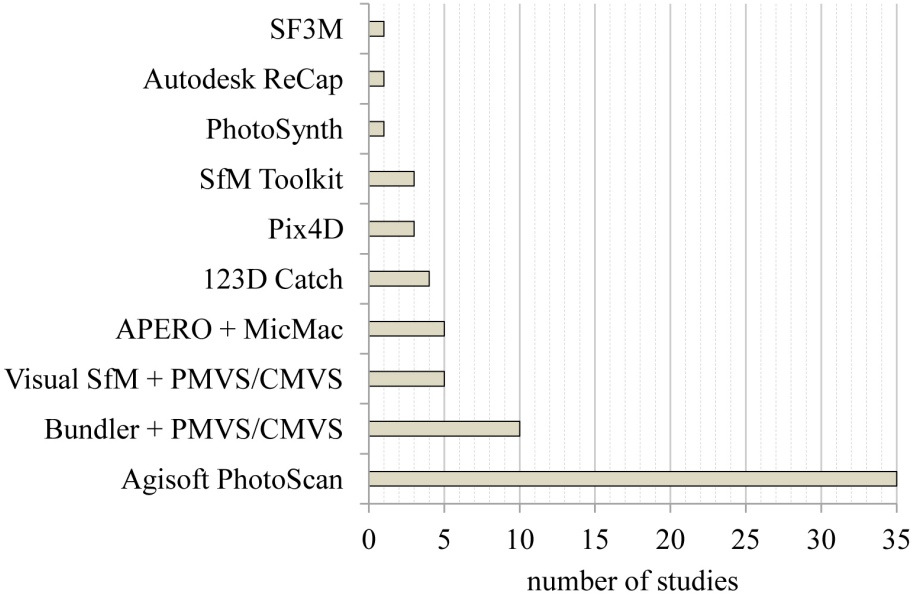

Figure 3. Variety of software used in the 62 reviewed studies.

ESURFD
3, 1445–1508, 2015

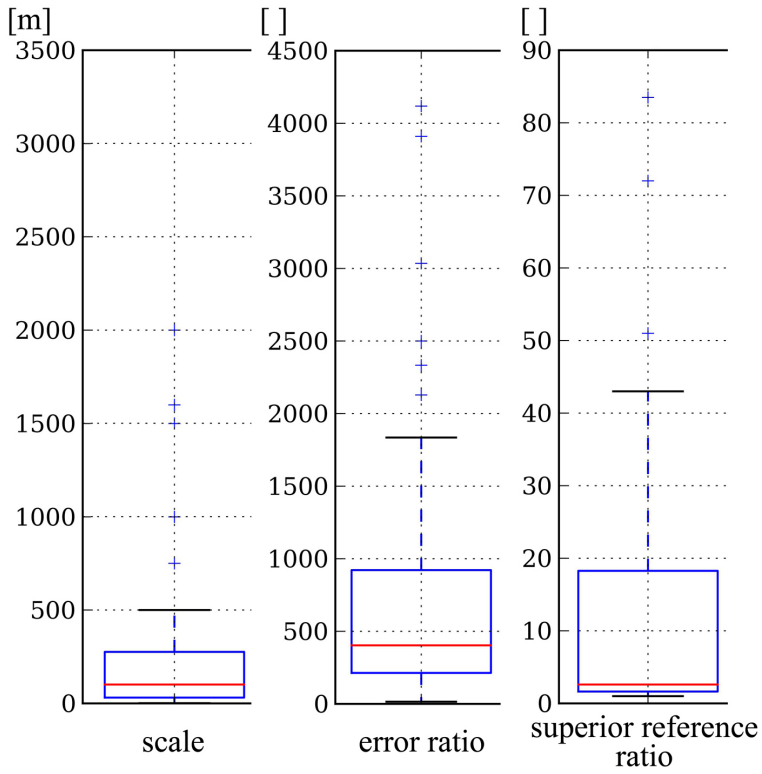

Figure 4. Boxplots summarizing statistics of scale, error ratio (calculated in regard to measured error and distance) and superior reference ratio (calculated in regard to measured error and reference error) of reviewed studies.

ESURFD
3, 1445–1508, 2015

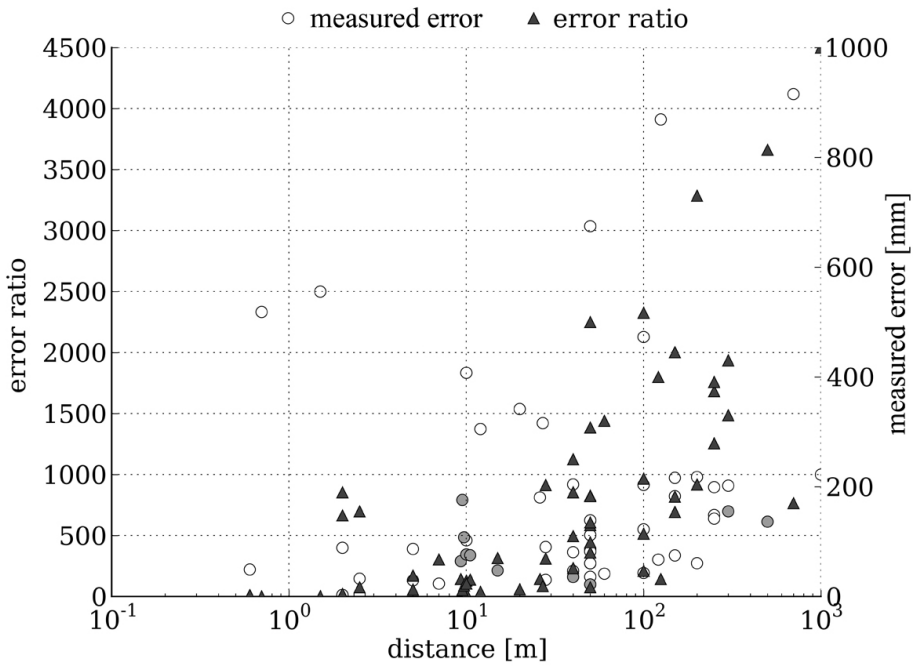

Figure 5. Relationship between measured error, error ratio and distance. For grey coloured points GCPs are measured in point cloud and for white points GCPs are measured in images for model transformation.

ESURFD
3, 1445–1508, 2015

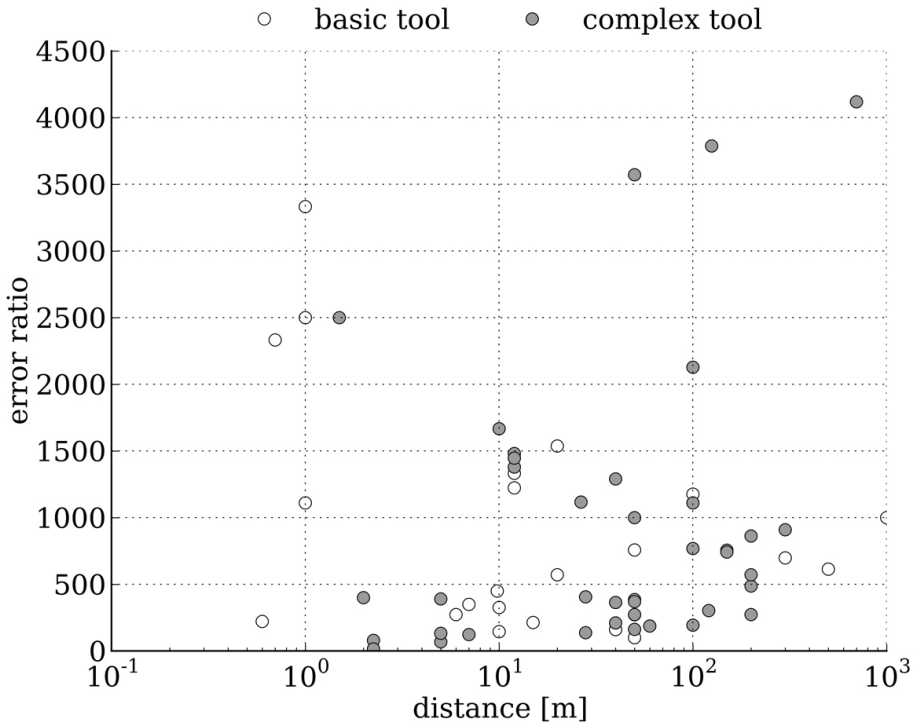

Figure 6. Image-based 3-D reconstruction performance of software considering basic and complex camera models.

ESURFD
3, 1445–1508, 2015

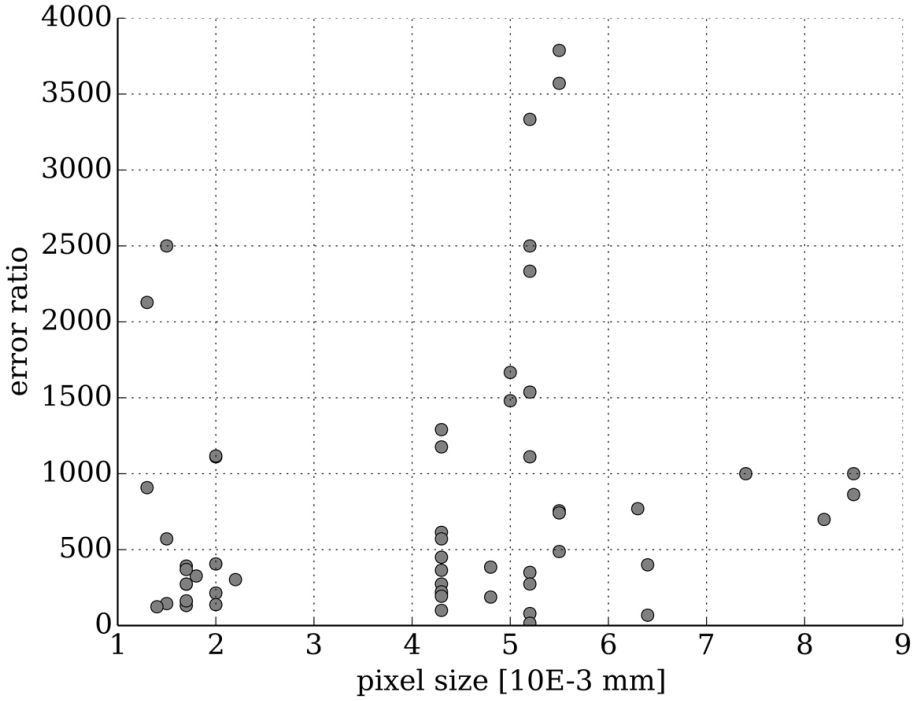

Figure 7. Influence of pixel size (and thus SNR) at the error ratio.

ESURFD
3, 1445–1508, 2015

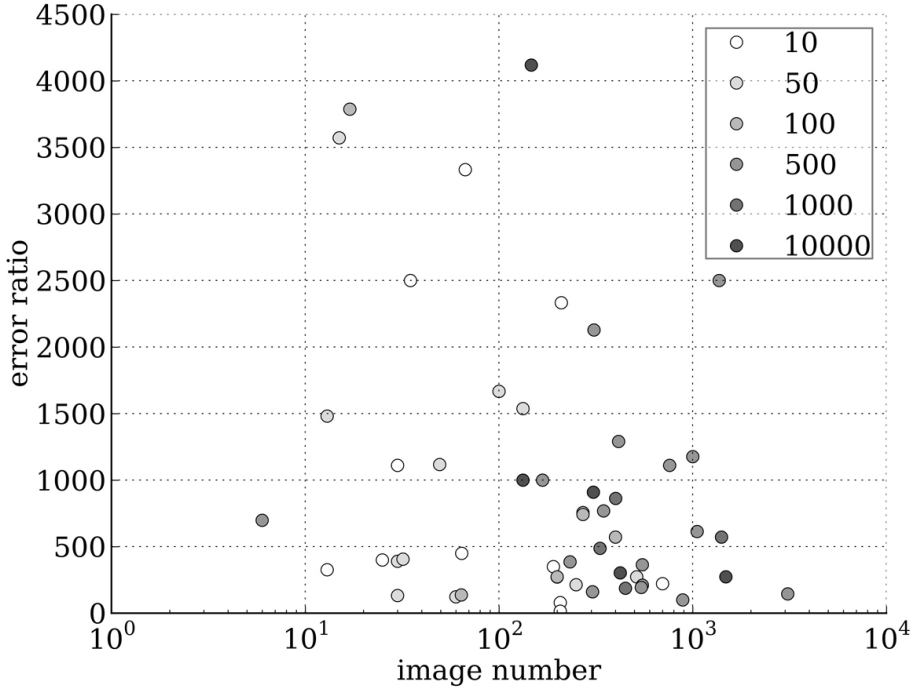

Figure 8. No distinct relation between error and amount of images detectable. Different scales are considered with point grey scales.

ESURFD
3, 1445–1508, 2015

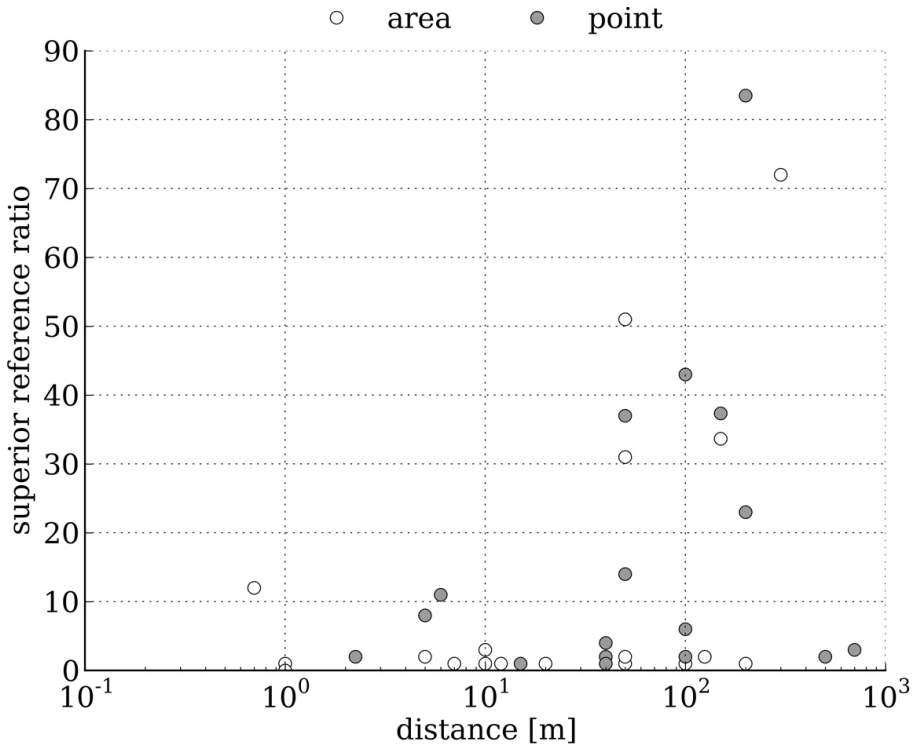

Figure 9. Superiority of the reference data. Superior reference ratio is calculated as ratio between measured error and accuracy of the reference. Area based and point based reference measurements are distinguished.

ESURFD
3, 1445–1508, 2015

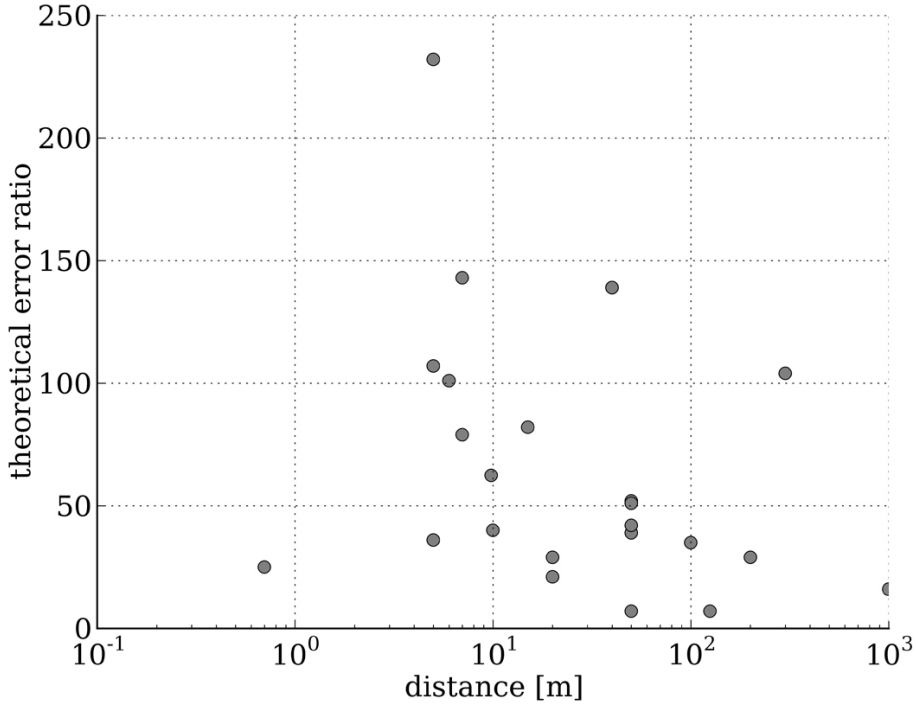

Figure 10. Ratio of the theoretical and measured error displayed against distance to illustrate image-based 3-D reconstruction performance in field applications.

ESURFD
3, 1445–1508, 2015

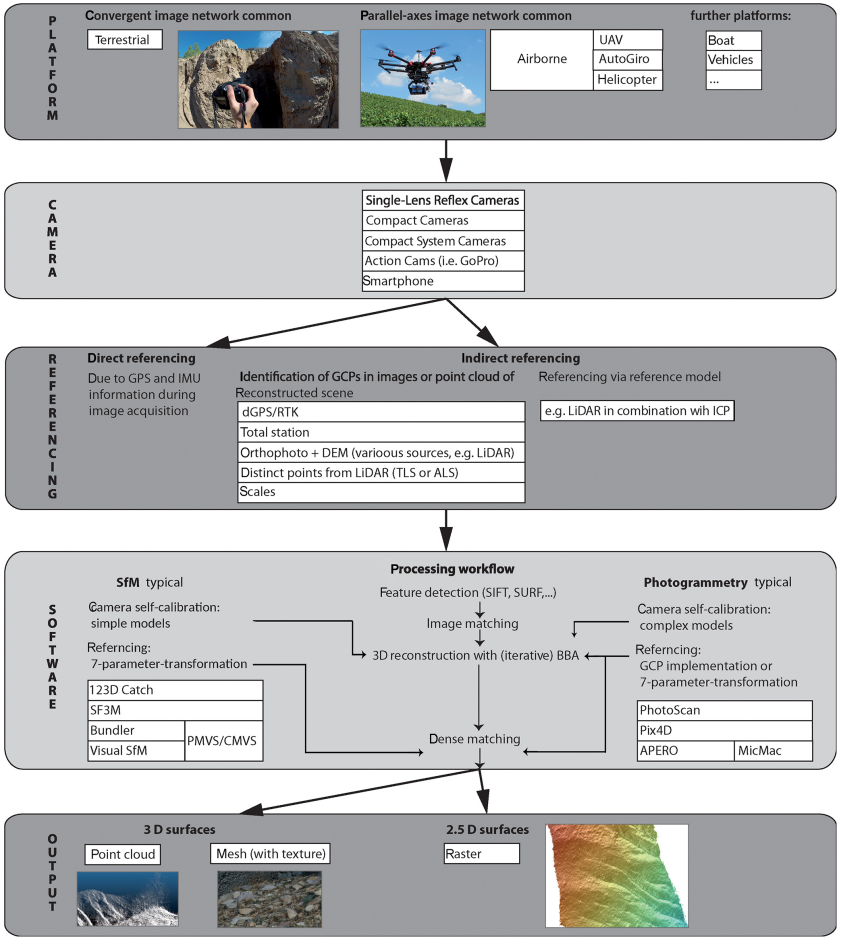

Figure 11. Schematic illustration of the versatility of SfM photogrammetry.

ESURFD
3, 1445–1508, 2015